UNIVERSIDAD DE SALAMANCA

FACULTAD DE BIOLOGÍA

Departamento de Bioquímica y Biología Molecular

STUDY OF THE INTERACTION OF THE MATRIX PROTEIN OF

THE NEWCASTLE DISEASE VIRUS WITH LIPID BILAYERS:

IMPLICATIONS FOR THE MECHANISM OF VIRAL BUDDING

ANNA SHNYROVA

2008

ENRIQUE VILLAR LEDESMA, CATEDRÁTICO DEL DEPARTAMENTO DE BIOQUÍMICA Y BIOLOGÍA MOLECULAR DE LA UNIVERSIDAD DE SALAMANCA

CERTIFICO:

Que la presente Tesis Doctoral titulada ¨**Estudio de la interacción de la proteína matriz del Virus de la enfermedad de Newcastle con bicapas lipídicas implicaciones en el mecanismo de la gemación vírica**¨, que para optar al grado de Doctora en Biología presenta Dña. ANNA SHNYROVA, ha sido realizada bajo mi dirección en el Departamento de Bioquímica y Biología Molecular de la Facultad de Biología de la Universidad de Salamanca.

Considerando que dicha tesis se halla concluida, autorizo su presentación para que pueda ser juzgada por el tribunal correspondiente.

Y para que así conste, firmo el presente certificado en Salamanca a 11 de Abril de 2008.

Dr. Enrique Villar Ledesma

To my painter…

ACKNOWLEDGMENTS

PREFACE

This thesis project has been carried out in the collaborative framework between the laboratory of Dr. Enrique Villar Ledesma from the University of Salamanca in Spain and the Laboratory of Dr. Joshua Zimmerberg from the National Institutes of Health in the USA.

This thesis has been partially published in the Journal of Cell Biology (JCB **179** (4), 627-633, (2007)) . Also, part of the thesis results has been communicated at the following International Meetings:

- Biophysical Society Meeting in 2006 and 2007, USA

- EMBO workshop on Cell Membrane Organization and Dynamics, 2006, Bilbao, Spain

- Thirteenth International Conference on Negative Strand Viruses, 2006, Salamanca, Spain

- International Conference "Membrane Biophysics of Fusion, Fission and Rafts in Health and Disease", 2007, Society of General Physiologists, Woods Hole, USA

ABBREVIATIONS

ANTS - 8-aminonaphthalene-1,3,6-trisulfonate
BLM – Bilayer Lipid Membrane
BODIPY - boron dipyrromethane difluoride
BSA – Bovine Serum Albumin
Ca^{++} - Calcium ion
COP – Coat Protein Complex
Corp. - Corporation
DOPC - 1,2-Dioleoyl-sn-Glycero-3-phosphocholine
DOPE - 1,2-Dioleoyl-sn-Glycero-3-phosphoethanolamine
DOPG - 1,2-Dioleoyl-sn-Glycero-3[pospho-rac-(1-glycerol)] (sodium salt)
DPX - p-xylenebis(piridinium bromide)
EM - Electron Microscopy
ER – Endoplasmic Reticulum
ESCRT - Endosomal Sorting Complex Required for Transport
F protein – viral fusion protein
FITC - Fluorescein isothiocyanate
GUV – Giant Unilamellar Vesicles
HIV - Human Inmunodeficiency Virus
HN protein - hemagglutinin-neuraminidase protein
HPAIV - highly pathogenic avian influenza virus
ILV - Intralumenal vesicles
Inc. – Incorporated
Lab. - Laboratories
L protein – Viral RNA polymerase
LUV – Large Unilamellar Vesicles
M protein – Viral matrix protein
MVB – Multivesicular Body
ND - Newcastle Disease
NDV – Newcastle Disease Virus
NP protein – Viral nucleoprotein
PAGE - Polyarylamide Gel Electrophoresis
PI – Phosphatidylinositol
POPC - 1-Palmitoy-l,2-oleoyl-sn-Glycero-3-phosphocholine
PS – Phosphatidylserine
Rh – Rhodamine
RNA – Ribonucleic acid
SDS – Sodium dodecyl sulfate
TEM –Transmitted Electron Microscopy
VLP – Virus-Like Particle

CONTENTS

"Where the world ceases to be the scene of our personal hopes and wishes, where we face it as free beings admiring, asking and observing, there we enter the realm of Art and Science."

Albert Einstein

I. INTRODUCTION

1.1. MEMBRANE BUDDING: FROM COMPLEXITY OF INTRACELLULAR TRAFFICKING TO THE RELATIVE SIMPLICITY OF VIRAL PARTICLE CREATION

1.1.1. Classical coated vesicles and novel membrane microdomains

Until the 1960's the eukaryotic cell membrane was considered a static structure. It was thought that the cell membrane's principal functions were to separate cellular contents within intracellular compartments and from external media, and to provide a template for protein reactions. In the mid 1960's George Palade and James Jamieson, during their electron microscopy (EM) studies on protein secretion, observed specialized invaginations in the plasma membrane (Jamieson and Palade, 1967a, b). The invaginations were covered by electron dense material on the cytoplasmic side, and moreover, vesicles with similar external coats were seen in close proximity to these invaginations, suggesting that these membrane structures are intermediates of the same process (Jamieson and Palade, 1967a, b). Inspired by these observations, the authors proposed what is now known as the vesicular transport hypothesis (Palade, 1975). This hypothesis states that molecules move from one subcellular compartment to another via shuttling vesicular transport (Bonifacino and Glick, 2004). Today we know that budding of membrane vesicles is ubiquitous in the life cycle of eukaryotic cells, where exocytic and endocytic transport vesicles are constantly generated to carry cargo and membrane components between different cellular compartments (Mallabiabarrena and Malhotra, 1995). These observations gave a new function to biological membranes as a dynamical component of the intracellular biochemical pathways which supports the bulk of the molecular transport and exchange. Thus, understanding the different mechanisms that cells use to perform and control vesicle budding is essential for understanding the fundamental principles of origin and life of eukaryotic cells (Svetina, 2007) (Figure 1).
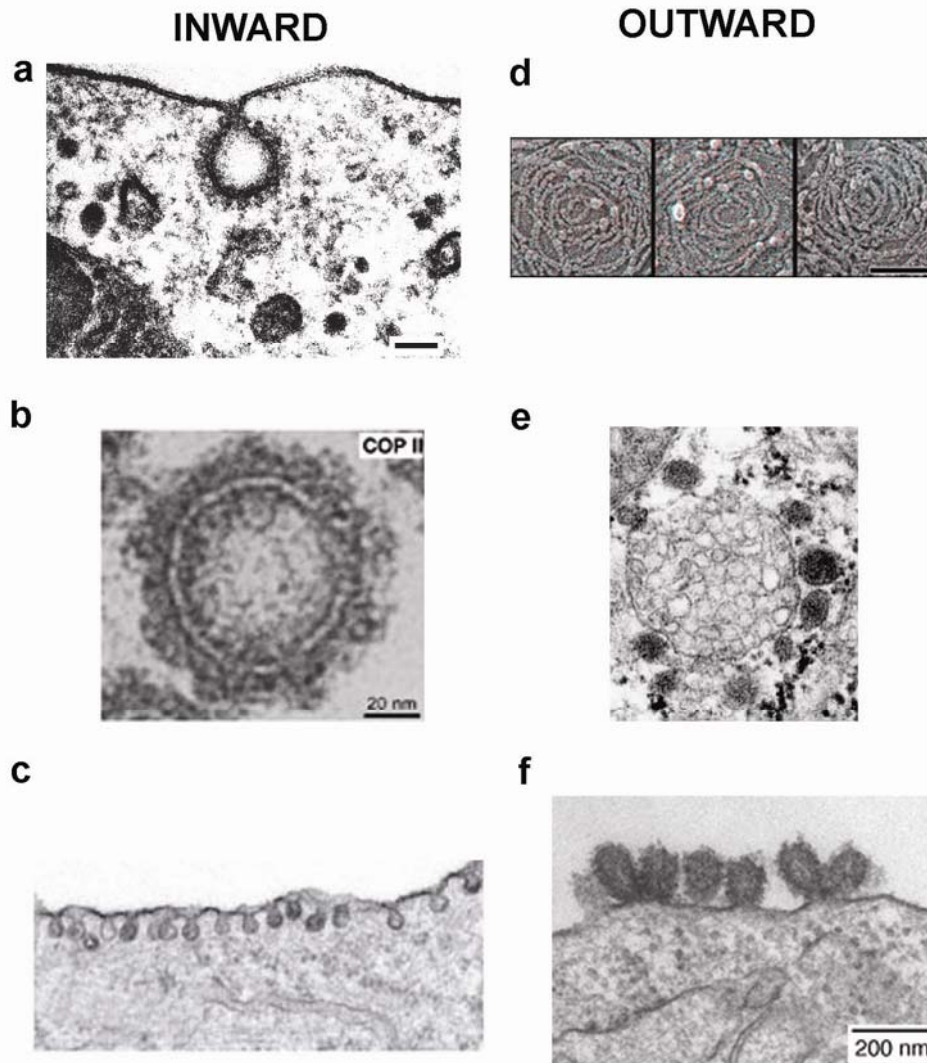
Figure 1. Types of cellular budding: electron microscopy imaging in cells. Inward cellular vesicle formations are shown in (**a**), where clathrin coated pits are seen with the clathrin lattice outside of the vesicle membrane (Marsh and McMahon, 1999) (bar 50 nm); in (**b**), where COP coated vesicle is shown[1] and in (**c**) where caveolae formation is represented (Parton and Simons, 2007). Outward vesicle formation is characteristic for MVB and viral budding. In MVB it is likely driven by the protein Snf7, which overexpression in cells gives rise to spiral-like structures formation on the plasma membrane as can be seen in (**d**) (Hanson *et al.*, 2008). The MVB formation may be observed in (**e**) (Stark *et al.*, 1988). Viral budding of many enveloped viruses is driven by their matrix protein (**f**) (Whittaker, 2001).

In the 1970s the vesicles visualized by Palade were isolated and the major component of their coat was identified as the protein clathrin. In the 1980s another type of coated vesicles was discovered: the COPI-coat vesicles were identified in the Golgi stack. In the 1990s COPII-coated vesicles were co-localized within the endoplasmic reticulum (ER) and were added to the list of vesicle protein coats (Robinson, 1997). Since clathrin's discovery, innumerable research papers and reviews have appeared talking

---

[1] Adapted from http://mol-biol4masters.org/Co_and_Post_Translational_Events5_Cellular_Protein_Traffic.htm

3

about the three *rigid scaffolds*[2] paradigm in vesicular trafficking (clathrin, COPI and COPII). Still, the molecular mechanism of the formation of coated vesicles has not been decoded completely because these vesicles are deeply involved in a great variety of protein and lipid networks. The enormous complexity lying behind the budding of coated vesicles is naturally related to the need for precise regulation of intracellular protein trafficking mediated by such vesicles.

However, basic principles underlying the creation of a spherical membrane geometry by protein coats are well understood. Both clathrin and COPII proteins produce basket-like structures in solution, demonstrating their intrinsic ability to self-assemble into spherical coats (Antonny *et al.*, 2003). On-membrane polymerization of a clathrin coat depends on membrane curvature, which is produced by adaptor proteins, such as AP180 or epsin, through amphipathic helix insertion into the outer leaflet of the lipid membrane (McMahon and Gallop, 2005). In the absence of adaptors, clathrin forms plane lattices which were observed by EM on a flat membrane surface (Ford *et al.*, 2002). Mechanisms underlying polymerization of spherical clathrin cages in the presence of adaptor proteins continue to be extensively studied (McMahon and Mills, 2004). The number of possibilities is growing exponentially as more and more adaptor proteins are discovered, each one bringing a new level of complexity into models describing the clathrin coat formation. Similar problems appear in the COP systems (McMahon and Mills, 2004). However, production of a rigid protein scaffold is not the only way that cells use to produce curvature needed for their functioning.

In 1953 Palade (and Enichi Yamada two years letter), discovered another type of highly curved membrane objects in cells: the caveolae (Palade, 1953; Yamada, 1955). Caveolae appear as structures resembling "*little caves*", which are vesicular invaginations of the plasma membrane 50-100 nm in size. It was only in 1992 when caveolin, the major protein component of caveolae, was identified and described as deeply inserted into the outer monolayer of the caveolae membrane (Rothenberg *et al.*, 1992). This discovery

---

[2] The term *rigid scaffold* or *rigid coat* is used in the recent literature to define a vesicle covered by a protein layer formed by oligomerization of proteins anchored to the outer monolayer of the vesicle membrane via partial insertion of a hydrophobic hub or via interaction with a membrane-inserted adapter-protein. When the rigidity of the clathrin scaffold was measured (Jin et al., 2006), it was found that the coat that clathrin forms in solution is close in rigidity to a plane membrane vesicle. Thus the hypothesis of a "rigid scaffold" imposing its intrinsic shape on a lipid membrane should be taken with caution.

allowed for a characterization of caveolae from chemical and biophysical points of view. Based on their lipid composition and topological behavior caveolae are considered to be a subtype of "membrane domains" that form invaginations and are capable of endocytosis and transcytosis (Couet *et al.*, 2001). The presence of a high amount of caveolin which is capable of inserting its hydrophobic hairpin-like domain inside the lipid matrix and forms a tight 1:1 complex with cholesterol (Martin and Parton, 2005), might indicate a new type of protein-lipid interaction within budding membrane domains. In this case the budding does not rely on multiple adaptors or signaling lipids, but on the interaction between protein molecules and protein-lipid moieties. Caveolin was not reported to form baskets in solution, so its ability to impose curvature is revealed only in the presence of the membrane matrix. The molecular basis of this new type of membrane deformation is yet to be elucidated, but it is logical to assume that the driving force of this new type of budding is hidden in the caveolin self-organization on a membrane surface.

Caveolin provides a new paradigm for curvature creation by proteins deeply embedded into lipid bilayer of cellular membrane where they form specialized budding domains transforming into invaginations and vesicles. In the last decade other proteins utilizing similar mechanisms of membrane remodeling have been discovered. They include the reggie/flotillins protein family characterized by a highly conserved prohibitin homology (PHB) domain which has a hairpin-like structure similar to the membrane domain of caveolins (Voeltz *et al.*, 2006). These proteins share other similarities: they generally partition into detergent resistant membranes, form oligomers, contain several phosphorilation sites and are typically localize in regions of high curvature (Bauer and Pelkmans, 2006). However, they also demonstrate interesting differences related to the dynamical properties of created membrane formations. Caveolins form relatively stable invaginations, caveolae, which usually consist of a cluster of vesicles indicating a difficulty in a vesicle detachment. Flotillins have been recently demonstrated to be more dynamic, producing large numbers of intralumenal vesicles (Frick *et al.*, 2007). This novel mechanism of vesiculation has been discussed broadly in the recent literature (Langhorst *et al.*, 2005).

It might be that caveolin and other membrane-embedded proteins interact with membrane lipids much more intimately that coat proteins. However, the last decade of

research on cellular membrane budding, both theoretical and experimental, has revealed lipids to be active participants of the budding process in general. To mention several examples, clathrin and COP assembly progress only if specialized charged lipids are present in the lipid membrane; especially important are the lipids of phosphatidylinositol (PI) family (McMahon and Gallop, 2005). Specialized lipids are involved in regulation of on-membrane association of membrane-embedded proteins, such as caveolin. This involvement is likely related to the ability of these molecules to form, transiently or constitutively, microdomains in the plasma membrane (Martin and Parton, 2005). Cholesterol is an important membrane molecule. Its ability to intercalate into the lipid bilayer and change various characteristics of the membrane together with its high concentration in some biological membranes, all suggest that cholesterol is one of the most important membrane moieties. For both, clathrin and caveolin dependent endocytosis, cholesterol's presence has been found to be a requirement (Baba *et al.*, 2001). However, it is not known whether cholesterol is transported to the budding sites by the proteins themselves or cholesterol-enriched membrane domains attract specialized proteins. The involvement of lipid microdomains in regulation of membrane curvature is actively studied.

1.1.2. Budding to the opposite direction: multivesicular body and viral budding

When thinking about vesiculation, the final topological organization of the vesicle should be taken into account. Members of both classes of curvature creating proteins presented above assemble onto the outer surface of the vesicle membrane. However, several cellular processes occur as a topological antipode of these mechanisms, i.e. proteins responsible for budding remain in the inner membrane monolayer, thus driving membrane budding in an outward direction (from the cytoplasm). This difference in directionality is directly related to the sign of the curvature created by the proteins: while coat proteins bend membranes with positive curvature (the sign is traditionally defined for the monolayer with bound proteins) the proteins inside a vesicle produce negative curvature. Two of the most representative examples of such a budding with negative

curvature are multivesicular body (MVB) formation and the budding of enveloped viruses.

The MVB consists of mid-stage endosomes containing hundreds of small (~50 nm) intralumenal vesicles (ILVs). The destiny of most of ILVs is in lysosomes, were their "cargo" of transmembrane proteins and lipids is degradated (Babst, 2005; Hurley, 2008). In recent years many proteins necessary for ILVs formation have been discovered. At least 18 members of the endosomal sorting complex required for transport (ESCRT) were identified as participants in ILV creation, though no definite mechanism unifying various interactions of these proteins and the process of ILV budding has been proposed (Hanson *et al.*, 2008). ESCRT proteins can be separated into three complexes, two of which are possible candidates for recruitment of the ubiquinated cargo that has to be recycled or degradated. The third complex, consisting of four proteins, is thought to promote the membrane bending and budding of ILVs itself (Hurley, 2008). As discussed early, proteins conducting membrane budding usually remain associated with the vesicle membrane. In the case of ESCRT pathway and ILV formation there has been no structural evidence for association of protein complexes with ILVs. Interestingly, Hanson and collaborators have recently shown that even without upstream regulatory factors, the overexpression in cells of Snf7, a protein from ESCRT-III, is enough to form uniform circular structures that can drive formation of buds and tubules (Hanson *et al.*, 2008) (Figure 1D). This indicated a new type of budding mechanism, where cooperativity between the protein and its coordinated action on the bilayer lipid membrane (BLM) leads to the formation of vesicles lacking any protein coat or lining.

Lipid analysis of MVB revealed the presence of a small amount of a very rare lipid, LBPA, which was shown to be able to promote budding of lipid membranes by itself, without protein involvement (Matsuo *et al.*, 2004). This lipid may appear in the late endosomes due to the action of some specialized enzymes, thus reversing the signaling and acting functions between lipids and proteins. On the other hand, phosphatidilinositols are required entities for the recruitment of ESCRT family proteins to the membrane during ILV formation (Hurley and Emr, 2006). It is interesting that different PI moieties are present during different stages of the endocytic pathway, thus indicating a very specific signal role for this charged lipid.

Budding of enveloped viruses is topologically similar to ILVs formation. Most non-enveloped viruses exit their host cells by lysis, which is a cell destructive mechanism. However, enveloped viruses chose another, more efficient, way of replication via membrane budding, where the integrity of the host cell membrane is preserved and the host is not necessarily killed (Welsch et al., 2007). Most viruses, such as retroviruses, alphaviruses, rhabdoviruses, and ortho- and paramyxoviruses, bud predominantly from the surface (plasma membrane) of the infected cell, but various intracellular organelle membranes were also shown to provide a platform for viral budding, thus resulting in the accumulation of viral particles in the lumen of such organelles (Welsch et al., 2007). Many viruses, like the Human Inmunodeficiency Virus-1 (HIV-1), may hijack cellular machinery to help themselves to egress (Chen and Lamb, 2008). In this way, for example, HIV was proposed to bud into the MVB of macrophages. However, recently, the role of intracellular compartments in HIV budding has been questioned and it has been proposed that the intracellular pool of viruses observed by EM mainly represents re-internalized particles that have originally budded from the plasma membrane (Jouvenet et al., 2006).

Whichever is the case, the notion that HIV and some other viruses interact with the members of the ESCRT machinery is now widely accepted, but there is no consensus about the exact role which ECSRT proteins play in virus formation (Chen and Lamb, 2008). One possibility is that ESCRT proteins participate in membrane fission in the terminal stage of viral egression. This hypothesis is further supported by the fact that ESCRT-related proteins were found to participate in another cellular process involving membrane division: the abscission during cytokinesis (Chen and Lamb, 2008). This finding may be an indication of a universal role for ESCRT proteins in cellular membrane fission finalizing inward membrane budding. If so, viruses may use the ESCRT machinery and the proteins known to disassemble the ESCRT III complex (the AAA-ATPase Vps4) to boost the efficiency of their budding. Nevertheless, this has not been demonstrated directly.

Despite possible interferences from a host cell, enveloped virus particles include only small traces of cellular proteins (Briggs et al., 2003), thus suggesting that this type of viruses ultimately rely on their own protein machinery for vesicle egression. Two principal mechanism of viral budding mediated by viral membrane proteins may be

distinguished. Budding can be led by viral transmembrane glycoproteins, shown to be sufficient for the formation of virus-like particles in the absence of any other viral component. This is the case for budding of viruses such as Influenza, Semliki Forest or Hepatitis B. Another mechanism of viral budding relies on the matrix proteins of the virus (Welsch *et al.*, 2007). Matrix protein is the major component of most enveloped viruses. This protein forms a tightly packed shell just beneath the lipid membrane of the virus, which resembles the caveolin coat of the endocytic vesicles, but with an opposite topology. Budding of most retroviruses (except Foamy Virus) and many paramixoviruses is exclusively driven by this *core protein*[3]. There are some exceptions where other viral proteins or other protein combination are the minimal requirements for budding (Welsch *et al.*, 2007).

The lipid composition of the cellular membrane can differ significantly from the viral one. It was proposed that some viruses bud selectively from membrane microdomains enriched by sphingomielin and cholesterol ("rafts"), as in the case of caveolin budding (Simons and Ehehalt, 2002). Lipidomics analysis of some viruses such as HIV (Brugger *et al.*, 2006) or influenza (Polozov *et al.*, 2008) indeed revealed a prevalence of raft-forming components: cholesterol, sphingomyelin and phospholipids with saturated side chains. However, as in the case of caveolin budding, is it not known whether those microdomains are virus-induced or preexisting in cell membranes.

In conclusion, all the budding processes that have been reviewed are based in protein-lipid interactions of different complexity levels, which lead to similar bending of the lipid matrix toward one preferential direction. Thus, to be able to understand the mechanisms behind the budding processes in cells, we have to take into account all the energy requirements to bend and bud a pure lipid membrane.

---

[3] In the case of retroviruses, matrix protein has been named Gag protein.

1.2. PHYSICAL-CHEMICAL PRINCIPLES BEHIND LIPID MEMBRANE BUDDING

1.2.1 Phospholipids and their polymorphism

Phospholipids are the major component of biological membranes. These molecules consist of a hydrophilic polar head group containing one or more phosphate groups and a hydrophobic tail, made up of two fatty acyl chains (Figure 2). The phospholipids polymorphism is exhibited in their ability to form different structures or phases through their aggregation into a monolayer (Epand, 2007). Such phases are often characterized by spontaneous or intrinsic curvature of the lipid monolayer defined as the curvature that a lipid monolayer adopts in solution in the absence of any external forces (Zimmerberg and Kozlov, 2006). Hence, lipids may be classified into three different classes based on the intrinsic curvature of the aggregated monolayer, which can be positive, zero or negative. For details and examples of the phases or shapes formed by the different phospholipids, see Table 1. The factors that determine the curvature preference are many. Among the most important ones are the lipid molecular structure, which will dictate the steric interactions between lipid head and acyl chains; hydrogen bonding or charge repulsions among head groups; hydratation of the lipid heads or temperature transitions, etc. (Epand, 2007). Phase transitions of several typical lipids are presented in Table 2.
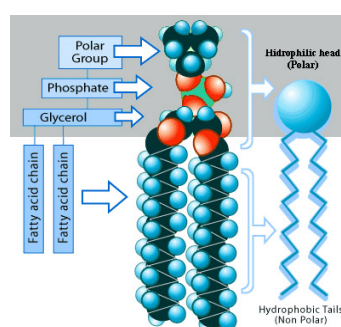
Figure 2. *Phospholipid structure.* Molecular and schematic representation of a phospholipid[4].

---

[4] Adapted from *www.bioteach.ubc.ca/Bio-industry/Inex/*
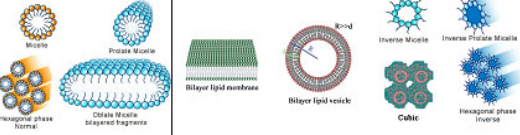
Spontaneous curvature of lipid mono-layer	Positive	Zero	Negative
Graphic representation of monolayer spontaneous curvatures	$J_S > 0$	$J_S = 0$	$J_S < 0$
Examples of lipids moieties that produce such curvature upon their aggregation into different phases at RT and physiological salt	Gangliosides; Lysophosphatidil-cholines (OPC, MPC, etc);	Phosphatidylcholines (DOPC, POPC, etc); Sphingomyelin; Phosphatilserines (DOPS, POPS, etc); Cardiolipin;	Ethanolamines (DOPE, POPE, etc.); Monoglucosyl-digliceride;
Examples of phases and shapes formed by monolayers of different spontaneous curvature	Micelle; Prolate Micelle; Hexagonal phase Normal; Oblate Micelle bilayered fragments	Bilayer lipid membrane; Bilayer lipid vesicle	Inverse Micelle; Inverse Prolate Micelle; Cubic; Hexagonal phase Inverse

Table 1. *Classification of the lipid monolayer spontaneous curvature and resulting phases.*

Lipid	Phase preferences Physiological conditions[b]	Other conditions
Phosphatidylcholine	L	H_{II}—low hydration and high temperatures
Sphingomyelin	L	
Phosphatidylethanolamine	H_{II}	L—pH $\geq$ 8.5 —low temperatures
Phosphatidylserine	L	H_{II}—pH $\leq$ 3.5
Phosphatidylglycerol	L	H_{II}—high temperatures and high salt concentrations
Phosphatidylinositol	L	
Cardiolipin	L	H_{II}—divalent cations —pH $\leq$ 3 —high salt
Phosphatidic acid	L	H_{II}—divalent cations —low pH $\leq$ 3.5 —high salt
Monoglucosyldiglyceride	H_{II}	
Diglucosyldiglyceride	L	
Monogalactosyldiglyceride	H_{II}	
Digalactosyldiglyceride	L	
Cerebroside	L	
Cerebroside sulphate	L	
Ganglioside	M	
Lysophosphatidylcholine	M	
Cholesterol		Induces H_{II} phase in mixed lipid systems
Unsaturated fatty acids		Induce H_{II} phase

L: lamellar or zero spontaneous curvature; H_{II}: inverse hexagonal or negative spontaneous curvature; M: micellar or positive spontaneous curvature.

Table 2. *Polymorphic phase preferences of unsaturated lipids* (Gruner *et al*., 1985)

As seen from Table 1, while in solution, lipids may form spontaneously not only planar bilayers (lamellar phase) characteristic for lipids such as DOPC, but also other

highly curved structures such as a micellelar phase (typical for lysolipids) or a hexagonal phase (as in case of DOPE). Hence, if a bilayer is formed from two monolayers the spontaneous curvature of the resulting bilayer[5] will depend on the spontaneous curvatures of the monolayers. Here three conditions may take place. a) If the bilayer is combined from two symmetrical monolayers with small and the same sign of spontaneous curvature, the resulting bilayer will be planar, due to mutual compensation of spontaneous curvatures of the monolayers. b) If the intrinsic curvature of the constituting monolayers is two high, the bilayer will not form at all, due to accumulation of curvature stress. c) If monolayers with two different spontaneous curvatures are combined, the resulting bilayer will have a spontaneous curvature with the sign of the monolayer with the more negative spontaneous curvature (Mouritsen, 2005) (Figure 3).
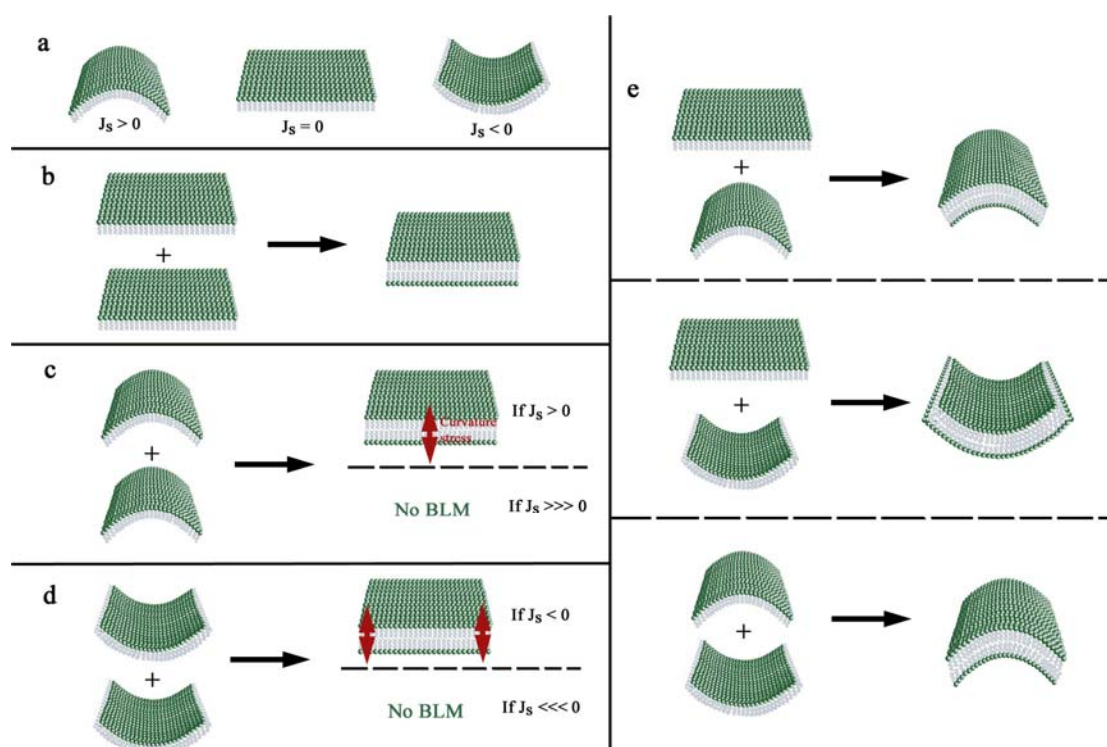
Figure 3. *Lipid bilayer curvature is dictated by the spontaneous curvature of its monolayers.* In **(a)** the three types of lipid monolayer curvature are represented. If a bilayer is formed from two of such monolayers, the following outcomes are possible: if two monolayers with zero curvature are combined, a lamellar phase will be formed, as can be seen in **(b)**. Two monolayers with the same positive curvature will also form a bilayer, however, if the intrinsic curvature of the monolayers is too high, the accumulated curvature stress will not allow for lamella formation **(c)**. The same situation is present in the case of two monolayers with same negative curvature **(d)**. If two monolayers of different curvature are combined, the resulting bilayer will have an average curvature as represented in **(e)**.

---

[5] Here we assume that the resulting bilayer is not a closed structure (such as a vesicle). Thus, the difference of the areas of the monolayers (area mismatch) is neglected.

The spontaneous curvature of the bilayer lipid membrane represents the initial state from which the budding may occur. The bending energy at this point is a minimum and to change this spontaneous membrane state work should be applied.

1.2.2. Energetics of membrane budding

Being a two dimensional liquid crystal, the bilayer lipid membrane has bending rigidity or stiffness opposing bending in the normal direction to the membrane plane (Zimmerberg and Kozlov, 2006). Thus, to produce a membrane bud certain forces should be applied to the membrane. Also, while transforming a "plane" membrane connected to a lipid reservoir (e.g. to a large membrane) into a "spherical" vesicle, there is an area increase, indicating that some lipids have to be transported to the budding site. This event also requires energy to work against the membrane lateral tension (Mouritsen, 2005). Thus, the requirement to deform a lipid membrane into a bud is to apply enough energy to overcome membrane resistance due to its bending rigidity and lateral tension. The energy related to the lateral tension of the membrane will depend on the bud area. The bending energy, having a more complicated nature, will depend on the initial and final states of the system, which needs to be defined in relation to the spontaneous and final curvature of the membrane.

1.2.2.1. Bending energy

The energy required to bend a membrane depends on the membrane curvature deviation from the spontaneous state of the system, in which the energy is equal to zero by definition. In a general case, this bending energy will depend on the two principal curvatures as follows:

$$E_{bend} = \frac{1}{2}k\int(\frac{1}{R_1} + \frac{1}{R_2} - 2C_{sp})^2 dA \qquad (1)$$

13

where C_{sp} is the spontaneous curvature of the membrane, R_1 and R_2 are the local curvature radii, A is the membrane area and k is the bending modulus (Helfrich, 1973). For typical phospholipid bilayers, $k \approx 20$ $k_B T$, where k_B is the Boltzmann's constant and T is the temperature expressed in degrees Kelvin. $k_B T$ (≈ 4.1 x 10^{-21} J) is the thermal energy (Reynwar *et al.*, 2007) and is frequently used to represent the energy requirements for a given process. When the formation of a spherical vesicle is considered, both curvature radii will be equal. This way, if zero spontaneous curvature is assumed, the total energy required to bend a membrane in order to form such vesicle will be independent of the radius of the vesicle (Reynwar *et al.*, 2007), as:

$$E_{bend} = \frac{1}{2} k \int (\frac{1}{R} + \frac{1}{R})^2 dA = \frac{1}{2} k (\frac{2}{R})^2 \times 4\pi R^2 = 8\pi k \approx 500 k_B T \qquad (2)$$

If this total bending energy is recalculated per lipid molecule in the area of geometrical transformation, it becomes clear that the process requires much more energy per molecule to produce small radii vesicles, than to produce larger vesicles. This way, the energy per lipid molecule required to create a vesicle of 50 nm in diameter will be approximately nine times bigger than the energy required to create a 150 nm vesicle. Thus, the protein action will be required to allow for the formation of the small vesicles that are characteristic for different cellular vesiculation processes. This way, the energy applied to the membrane during the polymerization of the clathrin "rigid" basket is of the same order of magnitude as the bending energy needed to produce a spherical vesicle with the typical diameter of a clathrin coated pit (Jin *et al.*, 2006). These similarity render the process of formation of vesicles by clathrin coating alone mostly probabilistic. Thus, the insertion of clathrin adaptors into the membrane leaflet induces the necessary spontaneous curvature of the membrane (Jin *et al.*, 2006) and considerably lowers the energy threshold.

As discussed above, lipids and proteins may induce membrane curvature by mechanisms other than bending by rigid scaffolds. The curvature can be imposed via alterations of spontaneous curvature of the monolayers by hydrophobic insertions (Zimmerberg and Kozlov, 2006). Spatial coordination of such insertions by attractive interactions mediated by membrane undulations creates membrane areas of increased spontaneous curvature (domains) that are prone to bud. Importantly, the ability of a

membrane domain to bud does not generally require alterations of the spontaneous curvature of the membrane. Domain budding is also driven by another force, line tension associated with the domain boundary (Lipowsky, 1992).

1.2.3. Domain structure of biological membranes and its role in membrane budding

The first step in understanding biological membranes was the development of the "fluid mosaic model" by Singer and Nicolson in 1972, which unified the findings and ideas of the preceding decade (Singer and Nicolson, 1972). In this model the lipids are seen as a sea in which many monomer proteins float unencumbered and the bilayer surface is exposed directly to the aqueous environment (Figure 4d). Although, this model became a standard conceptualization for membrane architecture, the ideas it represented are somewhat misleading. The idea that proteins are present at low concentration and dispersed in the lipid matrix has been questioned in the last decade; many studies showed a preferential association of protein molecules in the membrane plane (Engelman, 2005). Numerous findings during the last decades allowed for the emerging of the modern membrane concept where the membrane is seen with variable patchiness, variable thickness and higher protein occupancy than has generally been considered (Engelman, 2005) (an evolution of the biological membrane representations can be seen in Figure 4). Thus, the randomness of the two-dimensional liquid, presented by the "fluid mosaic model" has to be reviewed, and membrane fluidity has to be reconsidered with local organization into membrane patches or domains.

As described earlier, membrane lipids aggregate into different forms or phases. They, also, may undergo transitions between phases of different morphology that can be triggered by changing the water concentration under isothermal conditions (Mouritsen, 2005). In addition to this kind of transition, lipid aggregates, such as lipid bilayers, may undergo a number of internal phase transitions. These types of two-dimensional transitions are the basis of the formation of lipid membrane domains.
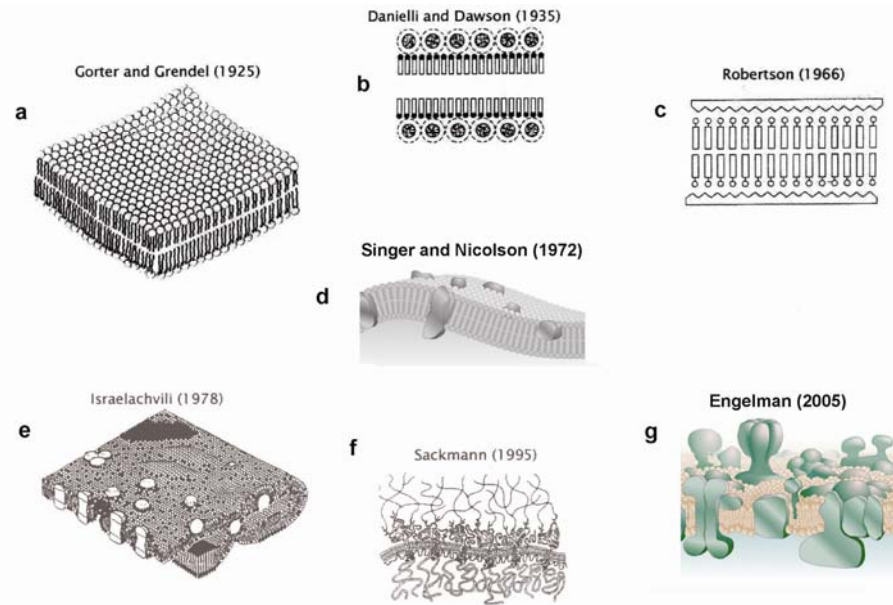
Figure 4. Historic picture gallery of membrane models (Mouritsen, 2005). **(a)**. Gortel and Grendel shown that the membrane is very thin, being only two molecules thick (Gortel and Grendel, 1935). **(b)**. The notion of the association of membrane proteins with the lipid bilayer was introduced by Danielli and Davson (Danielli and Davson, 1935). **(c)**. Robertson presented a related version of membrane organization, were membrane proteins are represented as layers sandwiching the lipid bilayer (Robertson, 1966). **(d)**. A standard conceptualization of membrane architecture as fluid-mosaic membrane was proposed by Singer and Nicolson in 1972 (Singer and Nicolson, 1972). **(e).** A refined membrane model was proposed by Israelachvili, where the need of membrane proteins and lipids to adjust to each other, pore formation, membrane folding, thickness variations and heterogeneity were took into account (Israelachvili, 1977). **(f)**. The importance of the cytoskeleton and glycocalix were introduced in the Sackmann's model (Sackmann, 1994). The latest version of the model, proposed by Engelman, can be seen in **(g)**, where the variable patchiness, variable thickness and higher protein occupancy than has generally been considered are represented (Engelman, 2005).

When more than one type of lipid molecules is present in a bilayer, the strong attraction interaction between species of the same kind may lead to the loss of translational mobility of the lipids (Mouritsen, 2005). As a result, a local transition from liquid phase (the fluid phase of the biological membrane) to a crystalline or solid phase occurs. When this new phase separates from the fluid phase of the membrane, the resulting membrane lipid domain may have a very different shape, but usually this domain is non-circular (Table 3). Another type of phase transition is intrinsic to the fluid phase of the membrane. This phase transition does not affect the translation motions of the lipid molecules, but produces long range ordering of the lipid tails. In this way a liquid ordered phase emerges. The result of this type of transition is the formation of circular domains which minimize their boundary energy, as will be discussed below

(Table 3). A general example of such liquid ordered domains is the lipid raft enriched in cholesterol and sphingomyelin. (Simons and Vaz, 2004).
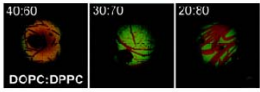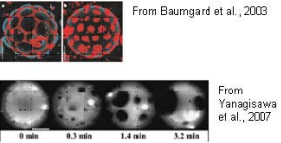
	Crystalline domains (crystalline and liquid phase coexistence)	Fluid-like domains (Liquid ordered and Liquid disordered phase coexistence)
	From Li and Cheng, 2006	From Baumgard et al., 2003 From Yanagisawa et al., 2007
Shape	Dependent of the polymerization pattern. Usually non-circular.	Circular. Tends to minimize boundary energy.
Domain evolution	Formation of complicated networks.	Fusion of domains to minimize perimeter
Bud size distribution	Sharp (?)	Broad

Table 3. *Crystalline versus Fluid-like domains* (Baumgart *et al.*, 2003; Li and Cheng, 2006; Yanagisawa *et al.*, 2007)*.*

Both, crystalline and liquid ordered domains embedded into the liquid disordered bilayer membrane, may lead to bud formation. In the case of the crystalline phase, membrane curvature may result from a tendency of the crystalline phase to grow in a direction normal to the membrane plane. However, this type of crystalline domain budding has not been observed in lipid systems. In contrast, the budding of lipid liquid ordered domains has been documented (Baumgart *et al.*, 2003).

In 1992, Reinhard Lipowsky proposed a new force responsible for the budding of fluid membrane domains (Lipowsky, 1992). He argued that a flat circular domain does not represent the state of lowest energy, since the length of the domain edge can be further reduced if the domain deforms into the third dimension and forms a bud (Figure 5). Lipowsky proposed a simple theoretical model, which predicted that liquid ordered domain should undergo budding as soon as it achieves to a certain limiting size and the edge energy of the domain becomes larger than the bending energy of the membrane. In his pioneering work Lipowsky made another important prediction: if the budding domain

is symmetrical (and, consequentially has zero spontaneous curvature), budding may proceed in both directions normal to the membrane plane. However, if the budding domain has non-zero spontaneous curvature, which implicates an asymmetrical distribution of compounds between the monolayers, budding will proceed toward one preferential direction dictated by the initial domain curvature.
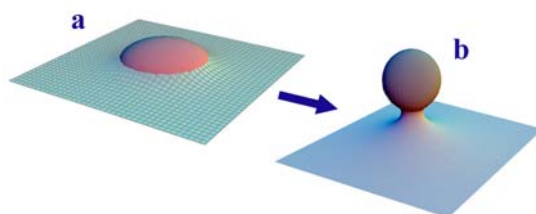
Figure 5. *Budding of a phase separated circular domain (red) embedded in the membrane matrix (blue).* The length of the domain edge decreases during the budding process from **(a)** to **(b)**[6].

These theoretical predictions can be directly applied to biological membranes. It is quite natural to assume that proteins can exercise control over the budding of fluid membrane domains. For example, the effect of a protein hydrophobic insertion into a lipid leaflet that changes the local curvature of that leaflet (McMahon and Gallop, 2005). However, if such proteins oligomerize on the membrane domain, the global curvature of the domain will be affected and the directionality needed in cellular processes will be granted (Zimmerberg and Kozlov, 2006). Other possible roles of proteins in the budding of membrane domains involve cholesterol segregation, which allows for the formation of such domains (Kirkham and Parton, 2005). Finally, proteins themselves are amphipathic moieties capable of forming monolayers (Boucher *et al.*, 2007) and, perhaps, segregate into fluid domains on the membrane surface.

These possibilities have not been explored well experimentally. The main limitation has been the lack of simple model systems that allows one to probe the role of different protein components involved in domain driven budding in cells. Such a system is expected to help identifying the molecular players and mechanisms of budding, as was successfully demonstrated in reconstituted model systems for "rigid" coats (Higgins and

---

[6] Partially adapted form Harden *et al.*, 2005

McMahon, 2005). Probably, one of the simplest budding event in a cell is the budding of an enveloped virus (for example, Newcastle Disease Virus) driven by its matrix protein. Thus, if other cellular mechanisms are not critical for the budding activity of this protein, the reconstitution of budding with the matrix protein in different model lipid system will lead to the understanding of the molecular mechanisms behind the viral budding and most likely will provide new insights into the mechanisms of cellular budding. The role of the membrane domain formation in the budding of enveloped viruses also may be verified using this kind of reconstitution systems, as the involvement of fluid-like lipid rafts in the budding of some viruses has been established (Simons and Vaz, 2004). Thus, the purpose of this work is to create a reconstituted model system(s) and to study the molecular mechanism of viral budding using matrix protein of NDV as a prototype budding agent.

1.3. NEWCASTLE DESEASE VIRUS AND ITS MATRIX PROTEIN

1.3.1. Newcastle Disease Virus: classification and characteristics

Newcastle Disease Virus (NDV) has been assigned by the International Committee on Taxonomy of Viruses (ICTV) to the genus 01.048.1.05, where 01 stand for order *Mononegativirales* (e.g. genome is not segmented and contains a single molecule of linear negative-sense, single-stranded RNA), 01.048 refers to the family *Paramixoviridae*, 01.048.1 refers to the subfamily *Paramixovirinae* and 01.048.1.05 to a recently formed genus of *Avulavirus*, which is represented by NDV and Avian Paramixoviruses[7]. The virus is roughly spherical, with a diameter between 150 to 500 nm; however the virus may appear as a filamentous particle of approximately 100 nm and variable length (Yusoff and Tan, 2001). The membrane envelop is derived form the host cell membrane. The virus has a negative-sense, single-stranded RNA genome which contains codes for an RNA-directed RNA polymerase (L), hemagglutinin-neuraminidase protein (HN), fusion protein (F), matrix protein (M), phosphoprotein (P) and nucleoprotein (NP) in the 5' to 3' direction (Alexander *et al.*, 1997) (Figure 6).
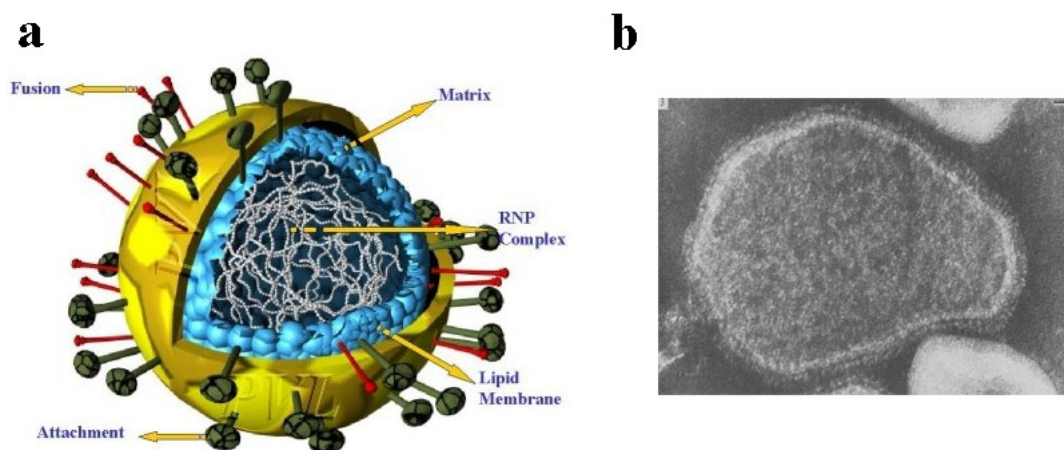
Figure 6. *Paramixoviridae structure.* **(a)** Three-dimensional image of Pneumovirus reconstruction originated by the University of Warwick, Pneumovirus Laboratory, UK. Matrix protein, shown in blue, orchestrates the virus formation. RNP complex attaches to the matrix core, which at the same time is associated to the lipid membrane and to the transbilayer glycoproteins such as the fusion protein[7]. **(b)** Real micrograph of a NDV particle after negative staining. Scale bar 25 nm (Russell and Almeida, 1984)**.**

---

[7] *ICTVdB - The Universal Virus Database*, version 4. *http://www.ncbi.nlm.nih.gov/ICTVdb/ICTVdB/*

All the steps of this virus replication cycle take place in the cytoplasm (Takimoto and Portner, 2004) (Figure 7). After the HN glycoprotein binds to its receptor on the cell surface, the F protein induces pH-independent fusion of the viral envelope with the plasma membrane of the infected cell. Then the viral nucleocapsid dissociates from the M protein core by an unknown mechanism and is released into the cytoplasm of the cell (Takimoto and Portner, 2004). The viral polymerase complex (P-L) transcribes each gene in the RNA template, and thus antigenome synthesis begins (Curran and Kolakofsky, 1999).
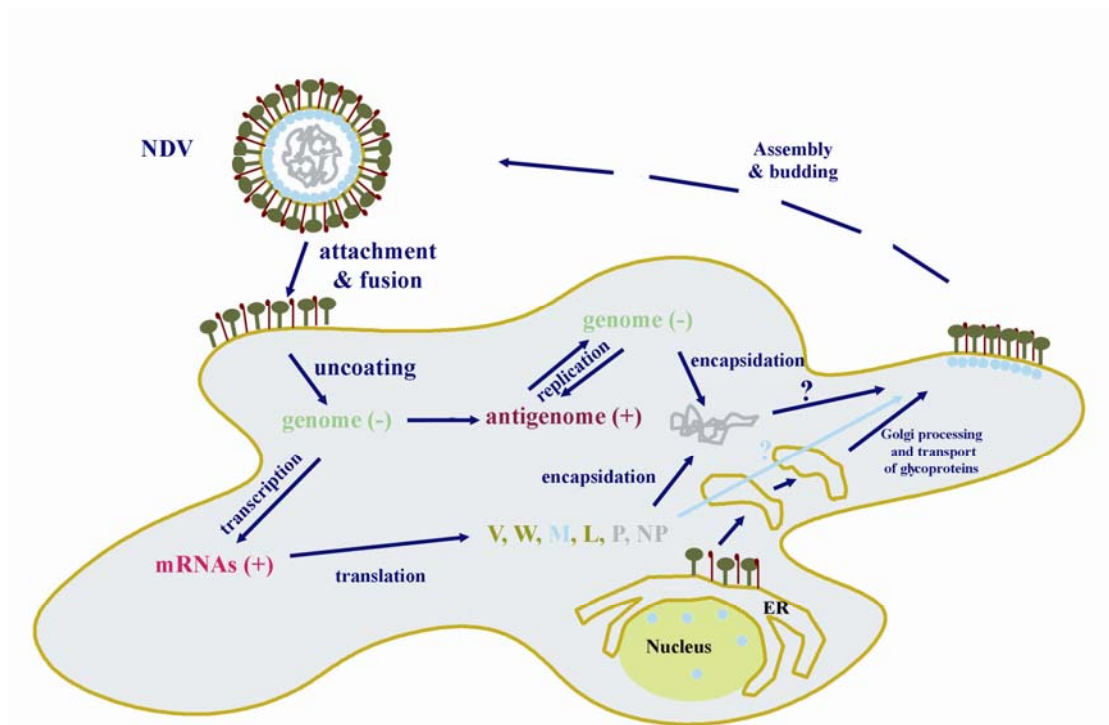
Figure 7. *NDV replication cycle.* Virions attach via specific receptors located on the surface of cell membrane and enter host cells via fusion of the viral envelope with the host cell plasma membrane in an environment of neutral pH. The viral genome is transcribed processively from the 3' end by virion-associated enzymes. The genome replicates in the cytoplasm. The parental genome does not serve as template; Replication is independent of the host nuclear functions. The assembly and egression of the virus is independent of the nucleocapsid (Yusoff and Tan, 2001).

Viral assembly takes place in the plasma membrane of infected cells, where M protein seems to have a key role (Takimoto and Portner, 2004). All the viral components, i.e. nucleocapsid, M protein, and envelope glycoproteins F and HN are transported to the plasma membrane where virions are assembled during the process of budding. The protein-protein interactions involved in assembly of the virion are very specific, with

other cellular proteins largely excluded from the final viral particle. M proteins clustering on the inner surface of the host cell's plasma membrane concentrate F and HN proteins as well as the ribonucleocapsid at the site of virus assembly (Takimoto and Portner, 2004). Interaction of M proteins with the cytoplasmic tails of the envelope glycoproteins is believed to be important for specific incorporation of the glycoproteins into the virion: mutation in the NDV matrix protein can result in decreased F protein incorporation into the particles and, thus, decreased infectivity (Peeples and Bratt, 1984). Moreover, the insertion of the viral genome into the virion is dependent on the interaction between matrix protein and the nucleocapsid complex. In this way, M protein presence at the budding site is a prerequisite for virus assembly (Yusoff and Tan, 2001).

Newcastle Disease virus is an avian virus that causes the Newcastle Disease (ND) in a wide host range with 27 to 50 orders of birds reported to have been infected (Alexander, 2000). This disease was discovered for the first time in East Indies in 1926, but it is named after Newcastle-upon-Tyne, England, where it was rediscovered a year later in 1927. Since 1927 this virus was responsible for many severe epidemics that caused death to thousands of wild and domestic birds, together with the economical impact to the poultry industry (Lomniczi *et al.*, 1998). The virulence varies with virus strain. Accordingly, NDV strains may be classified into lentogenic or low virulence viruses, that cause mild respiratory or enteric infections; mesogenic strains or intermediate virulence, that cause respiratory or nervous signs with moderate mortality; and velogenic strains, that cause severe intestinal and/or neurologic disease resulting in fast and high mortality (Seal *et al.*, 2000).

NDV is closely related to human paramixoviruses such as measles, mumps, human parainfluenza or respiratory syncytialvirus and distantly related to the lethal filoviruses, Ebola, Marburg or Rabies virus[8]. But surprisingly, NDV causes only minor illness in humans, limiting its manifestation to mild conjunctivitis and mild influenza-like symptoms. Moreover, this virus has certain characteristics that make it suitable for therapeutic applications. Recently NDV was proposed as a promising vaccine against the highly pathogenic avian influenza virus (HPAIV), which has a 60% mortality rate in the

---

[8] Samal, S; NIH personal communication located at:
http://www.webconferences.com/nihoba/ppt/Newcastle%20Disease%20Virus_Samal.pdf

22

human population (DiNapoli *et al.*, 2007). The development of vaccines against this virulent virus were impeded due to its low immunogenicity, the high quantities of killed vaccine required, and risk of genetic exchange of a live vaccine with circulating influenza virus strains. Thus, NDV appeared as a perfect candidate for this vaccine, due to its negligible incidence of recombination. In their recent work, DiNapoli and coauthors used recombination genetics to generate a recombinant NDV as vaccine against HPAIV. They demonstrated reduction or complete prevention of transmission of the HPAIV virus in monkeys (DiNapoli *et al.*, 2007). Although this result is of great interest, the use of a virus as a vaccine against another virus should be taken with extreme caution, as the exact mechanisms of cell and viral cycles are not yet well established (Han *et al.*, 2008)[9].

NDV has been the object of another type of breakthrough study, where its ability to replicate 10,000 times faster in tumor cells versus normal cells was explored (Adams and Prince, 1957). NDV oncolytic properties were discovered in the late 50s, and since then, NDV was actively studied as a potential antitumoral agent (Horvath *et al.*, 1999). Viral oncolytic therapy has two principal ways of application: one is an indirect increase of antitumor immunity through a modulation of the immune response and another is a direct treatment of tumors with replicating, oncolytic viral vectors. In this aspect, reverse genetic technology enables generating recombinant NDV strains with therapeutic genes encoded to enhance the oncolytic properties inherent to some native NDV strains (Janke *et al.*, 2007; Vigil *et al.*, 2007; Puhler *et al.*, 2008). As a result, tumor cells begin to express the apoptotic or danger signals what stimulate the activation of the immune-system response against this infected cells. In the direct oncolytic mechanism, however, the natural viral cycle results in complete lysis of host cells. This cycle can then repeat itself with the progeny virion infecting adjacent tumoral cells and destroying them by replication (Mullen and Tanabe, 2002). Thus identification of the proteins responsible for NDV formation and budding and a deeper understanding of the budding mechanism are becoming necessary to understand and further develop this type of viral oncotherapy.

---

[9] In the recent article by Han and coauthors, the widely accepted notion that NDV lack recombination was questioned. The authors found a new natural multi-recombinant strain of NDV, the result of a combination of at least three another known strains, one of them used as a vaccine for poultry.

1.3.2. Matrix protein of Newcastle Disease virus: its known and unknown properties

As mentioned above, matrix proteins of different negative-strand RNA viruses play a key role in the assembly and budding of the virions (Garoff *et al.*, 1998; Takimoto and Portner, 2004). NDV matrix protein was proposed to orchestrate the virus assembly by interacting with the nucleocapsid protein (NP), regions of the transmembrane glycoproteins (the F-HN complex) and lipid bilayer (Yusoff and Tan, 2001).

Unfortunately, the tertiary structure of NDV M protein has not been resolved yet, but its gene has been sequenced by Philip Chambers and coauthors in 1986 (Chambers *et al.*, 1986). The authors showed that this protein consists of 364 amino acids, which corresponds to a polypeptide with a molecular weight of approximately 40 kDa. This protein contains 8% acidic and 14% basic amino acids. M protein has a net charge of +19.5 at pH 7.0, assuming a charge of +0.5 for the histidine residues. However, the basic residues are not uniformly distributed along the sequence, giving the N terminus of the protein an acidic character due to the presence of 100 somewhat acidic amino acids in this region (Chambers *et al.*, 1986). Thus, its basic and acid charge distribution can mediate electrostatic interactions between different viral components, such as neighboring matrix proteins (Sagrera *et al.*, 1998), the virus spike formers F and HN glycoproteins (Peeples and Bratt, 1984; Garcia-Sastre *et al.*, 1989), or, the RNP complex from the virus interior (Garoff *et al.*, 1998). The same electrostatic forces were reportedly involved in the interaction of M protein and a cellular protein actin, present in small quantity in the NDV virion and other enveloped viruses (Giuffre *et al.*, 1982; Han and Harty, 2005). Actin filaments of the cell cytoskeleton may be the railways by which the virus transports its M proteins through the cytosol to the plasma membrane surface, as was shown recently for Gag protein from equine infectious anemia virus (Chen *et al.*, 2007).

NDV M protein interacts non-electrostatically with lipid membranes. The non-electrostatic character of M protein-lipid membrane interaction has been confirmed by protein binding to artificial liposomes, where no sensitivity to the presence of positively or negatively charged lipids in the membrane (such as stearylamine or PS) or ionic strength of the surrounding buffer was detected (Faaberg and Peeples, 1988). A hydropathy plot of the primary structure of NDV M protein revealed that M protein has a

hydrophobic character, but there is no region large enough to span the lipid bilayer; this is in good agreement with the location of the protein on the inner surface of the viral envelope (Li *et al.*, 1980; Chambers *et al.*, 1986). Strong hydrophobic M protein interaction with the lipid membrane was further showed to restrict the degree of rotation of lipid moieties in the membrane (Neitchev and Dumanova, 1992). Thus, M protein exhibits strong nonspecific binding to artificial lipid bilayers.

However, this lack of lipid specificity is not reflected in the lipid composition of the virus, where enrichment of certain component, such as cholesterol or sphingolipids, has been observed (Laliberte *et al.*, 2007). This suggests that membrane binding and membrane bending by M protein is not in a direct relationship, and/or that viral glycoproteins participate in the process of lipid selection *in vivo*. In relation to this, it was recently shown that the incorporation of functional HN-F complexes into NDV is dependent on the presence of cholesterol (Laliberte *et al.*, 2007). Furthermore, the presence of traces of caveolin and flotillin, both having high affinity for cholesterol, in NDV particles was reported (Laliberte *et al.*, 2007). How cholesterol is concentrated in the NDV envelop is still to be determined. To mention some possibilities, M protein may act as caveolin, concentrating the cholesterol in the budding sites, actin filaments may bring M protein to cholesterol enriched domains on the plasma membrane or viral glycoproteins might be delivered to the budding site in cholesterol-enriched domains.

The ability of matrix proteins of different enveloped viruses to form Virus-Like particles (VLPs) when expressed in cells has been known for some time (Jayakar *et al.*, 2004; Takimoto and Portner, 2004). For NDV, VLP formation was shown recently (Pantua *et al.*, 2006), when expression of M protein alone or in combination with NP, F and HN gave resulted in VLP formation (Figure 8). Any viral protein combination expressed in the absence of M failed to produce VLPs. This confirms the key role of M protein in the assembly and its requirement for the budding of NDV and other enveloped viruses.
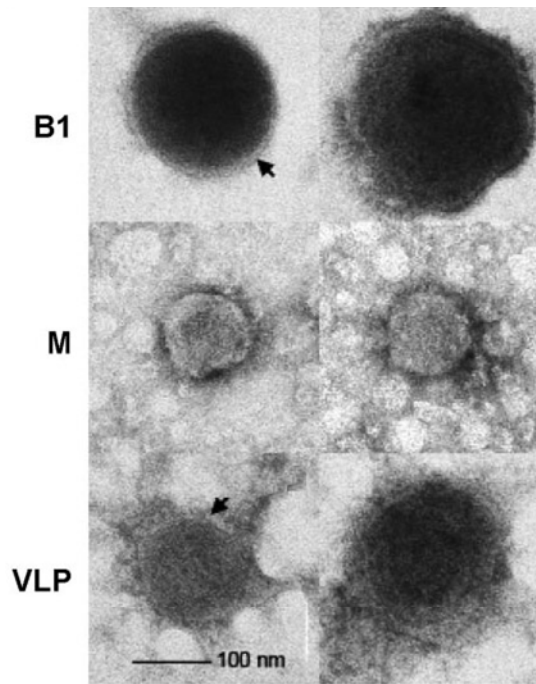
Figure 8. *Electron microscopy images of different particles formed by NDV proteins expressed in cells.* Particles from NDV infected cells (B1), M protein-expressing cells (M), or cells expressing NP, M F and HN proteins can be observed (Pantua *et al.*, 2006). As can be seen, all the particles are of similar shape and size, thus confirming the requirement and sufficiency of M protein in the budding of NDV.

Brought together, the strong lipid binding and the ability to produce VLPs in cells indicates that M protein possesses the energy and the functionality necessary to induce unidirectional membrane curvature and, possibly, membrane neck fission. However, as discussed previously, cellular components may also support M protein budding action. At this point, the proposed study of M protein interactions with model membrane systems should clarify the mechanism of membrane budding and establish a common pathway for the budding of some enveloped viruses.

1.4. Objectives

In the last 50 years, the knowledge of the mechanisms of cellular membrane budding has been dramatically expanding. However, a deep understanding of the physical principles and molecular mechanisms of membrane rearrangements during the budding is still lacking. So far, we have identified many players, but we are just starting to elucidate the rules of the game. The best way to progress in this understanding is by using the simplest system and by trying to extend the knowledge obtained with such a system to more complicated ones. From this point of view, viral budding is, probably, the best candidate to start with. Although, viruses may sequester the cellular machinery to vesiculate more efficiently, their budding is not as tightly controlled as in the endocytic or endosomic case. Viruses have limited amount of proteins, making it easy to study protein interactions in depth. Moreover, as described above, it is already known that many viruses rely only on one protein for their budding. Also, studying virus budding is of great interest to cell biology, as the identification of viral proteins involved and the mechanisms that viruses utilize to exploit cellular processes is expected to yield important insights in our understanding of the cell. Furthermore, the understanding of molecular mechanisms and the main driving forces of viral budding can suggest new methods to interfere with virus release, thus having therapeutic uses against virus infections (Welsch *et al.*, 2007). All these considerations made the viral budding a perfect candidate for the present study.

Thus, the main purpose of this work is to create a reconstituted model system(s) to study the mechanism of viral budding using matrix protein of NDV as a prototype budding agent. With this general purpose, the following specific objectives were established:

- *Purification of functional matrix protein from NDV*
  - Obtaining matrix protein with high purity
  - Designing lipid membrane systems to characterize the membrane activity of the purified protein (e.g. binding and curvature creation)

- *Development of a model lipid system which allows reconstitution and real-time monitoring of domain-driven budding by the matrix protein*

27

- o Visualization of protein induced budding on giant unilamellar vesicles using bright-field and fluorescence microscopy
- o Characterization of budding dynamics by electrophysiological approaches on planar bilayer lipid membranes

- *Characterization of molecular mechanisms of budding*
    - o Study the influence of lipid composition
    - o Study the membrane self-assembly of M protein on membranes and monolayers

An experiment is a question which science poses to Nature, and a measurement is the recording of Nature's answer.

Max Planck

II. MATERIALS AND METHODS

2.1. APPARATUS AND MATERIALS

Centrifuges:

 - J2-21 centrifuge (Beckman Coulter Inc., USA)

      Rotors: JA-14 angular rotor

- Optoma XL-100K ultracentrifuge (Beckman Coulter Inc., USA)

      Rotors: SW-28 rotor, 50.2 Ti angular rotor and SW 55Ti (Beckman Coulter Inc., USA)

- Eppendorf Centrifuge 5415D (Eppendorf, USA)

- Bottles, tubes and vials appropriate for each type of rotor

SDS-PAGE:

- Novex® 4-20% Tris-Glycine precasted gels 1.5 mm X 10 well (Invitrogen^{TM} Corp.,USA)

- XCell SureLock™ Mini-Cell Electrophoresis System (Invitrogen^{TM} Corp.,USA)

- PowerPac™ Basic power supply (Bio-Rad Lab., USA)

- FluorChem® FC system (Alpha Innotech Corp., USA)

Protein concentration analysis

- BCA™ protein assay kit (Pierce Biotechnology, Inc., USA)

- SpectraMax 250 microplate reader (Molecular Devices Corp., USA)

- Bio-Mini DNA/RNA/Protein analyzer (Shimadzu Scientific Instruments Inc., USA)

LUV preparation:

- Thermobarrel Extruder (Lipex Biomembrane Inc., Canada)

- Polyester drain discs (Osmonic Inc., USA)

- Polycarbonate 0.1 micron size filter (Osmonic Inc., USA)

- Sephadex™ PD-10 columns (GE Healthcare Life Sciences, USA)

- Superose™ 6 prep grade (GE Healthcare Life Sciences, USA)

- 1.5x30 cm Econo-Column® Chromatography column (Bio-Rad Lab., USA)

- N4 Plus Submicron Particle Sizer (Beckman Coulter Inc., USA)

GUV preparation

- Function generator GFG-3015 (Instek, USA)

- 1 mm diameter platinum wire (Goodfellow Corp., USA)

Microscopy:

- 0.17 mm thick Delta T Dish (Bioptech Inc., USA)

- Axiovert 200 Inverted microscope (Carl Zeiss, Inc., Germany):

- 40x, 0.75 NA objective (ACHROPLAN; Carl Zeiss, Inc., Germany)

- 150x, 1.45 NA objective (Olympus America Inc., USA)

- CoolSNAP EZ camera (Photometrics, USA)

- IPLab acquisition software (BioVision, Inc., USA)

- IX-70 inverted microscope (Olympus America Inc., USA)

- 150x, 1.45 NA objective (Olympus America Inc., USA).

- Intensified charge-coupled device camera VE1000SIT (Dage-MTI, USA)

- Metamorph Flashbus acquisition software (Molecular Devices Analytical Technologies, USA)

- Tecnai G2 transmission electron microscope (FEI Company, USA)

- 300 mesh carbon-coated gold EM grid (Electron Microscopy Sciences, USA)

Protein thiol groups labeling

- HiTrap™ desalting columns (GE Healthcare Life Sciences, USA)

- Model 2110 fraction collector (Bio-Rad Lab., USA)

Electrical admittance measurements:

- Flaming Brown Micropipette puller; Model P80/PC (Sutter Instruments Co., USA)

- 1.5 mm capillary borosilicate glass with filament (World Precision Instruments Inc., USA)

- MicroFil™ syringe needle (World Precision Instruments Inc., USA)

- Teflon® film (Fluoro-plastics, Inc., USA)

- Red Sable brush #00 (Da Vinci brushes, USA)

- Ag/AgCl pellet electrodes #EP05 (World Precision Instruments Inc., USA)

- ESA-CSA Piezo micromanipulators (Newport Corp., USA)

- EPC 7 patch clamp amplifier (HEKA Instruments Inc., USA)

- PC-44 acquisition board (Signalogic, USA)

- Bronew adquisition software (Ratinov *et al.*, 1998)

Other apparatus and materials used:

- Aminco-Bowman Series-2 luminescence spectrometer (Thermo Electron Corp., USA)

- MicroTrough S (Kibron Inc., Finland)

- 25 mL gradient mixer (Sigma-Aldrich Corp., USA)

- Dynamax peristaltic Pump (Rainin Instrument, LLC, USA)

- PC workstations (Dell Inc., USA)

- Slide-A-Lyser® Dialysis Cassette; 10,000 mw; 3-12 mL (Pierce Biotechnology, Inc., USA)

- Homemade and specially designed teflon chamber for monolayer formation and protein application

- Rocker II orbital shaker (Boeker Scientific, USA)

- Savant SpeedVac® Concentrator (Thermo Scientific, USA)

- Stirrer/hot plate (Corning Inc., USA)

- Vortex-genie 2 mixer (Scientific Industries Inc., USA)

- PM 4600 Delta Range® scale (Mettler-Toledo, Inc.)

- Balance (Sartorius AG, Germany)

- Orion pH meter model 420A (Thermo Scientific, Inc, USA)

- Safeaire fume hood (Fischer Hamilton, USA)

- Vapor pressure osmometer 5500 model and calibration solutions (Wescor Inc., USA)

- Freezers (-30 and -80) and fridge (4ºC) (Revco, Thermo Scientific, USA)

- Argon, compressed gas (NIH supply service)

- Nitrogen, compressed gas (NIH supply service)

- Liquid nitrogen (NIH supply service)

2.2. CHEMICALS AND LIPIDS

Lipids

- Dioleoylphosphatidylcholine, DOPC (Avanti Polar Lipids, Inc., USA)

-1-palmitoyl-2-oleoylphosphatidylcholine, POPC (Avanti Polar Lipids, Inc., USA)

- Dioleoylphosphatidylethanolamine, DOPE (Avanti Polar Lipids, Inc., USA)

-1,2-dioleoyl-phosphoglycerol, DOPG (Avanti Polar Lipids, Inc.,USA)

- DOPE–lissamine Rhodamine B sulfonyl, Rh-DOPE (Avanti Polar Lipids, Inc., USA)

- Cholesterol (Avanti Polar Lipids, Inc.,USA)

- G_{M1} ganglioside conjugated with BODIPY-FL (Invitrogen[TM] Corp., USA) in the polar head region, BODIPY-G_{M1}, was synthesized as described previously (Samsonov *et al.*, 2001).

Dyes

- 8-aminonaphthalene-1,3,6-trisulfonate, ANTS (Molecular Probes™ Invitrogen™ Corp., USA)

- *p*-xylenebis(piridinium bromide), DPX (Molecular Probes™ Invitrogen™ Corp., USA)

- 70 kDa Fluorescein isothiocyanate conjugated dextran, FITC-dextran (Sigma-Aldrich Inc., USA)

- Uranyl Acetate (Electron Microscopy Sciences, USA)

- Cy3 maleimide mono-reactive dye (GE Healthcare Life Sciences, USA)

SDS-PAGE

- Tris-Glycine SDS sample Buffer (2x) (Invitrogen[TM] Corp.,USA)

- NuPAGE[®] Reducing Agent (10x) (Invitrogen[TM] Corp.,USA)

- SeeBlue® Plus2 Prestained Standard (1x) (Invitrogen[TM] Corp.,USA)

- Novex[®] Trys-Glycine SDS Running Buffer (10x) (Invitrogen[TM] Corp.,USA)

- SimplyBlue™ SafeStain (Invitrogen[TM] Corp.,USA)

- SYPRO[®] Ruby protein gel stain (Invitrogen[TM] Corp.,USA)

Gradients components

- Di-potassium tartrate hemihydrate (Fluka, Sigma-Aldrich Corp., USA)

- Ficoll® PM400 (GE Healthcare Life Sciences, USA)

Buffers and buffer components

- Tris-HCl 1 M solution pH 8.0 (KD Medical, Inc., USA)

- Sodium chloride (NaCl) 5 M solution (KD Medical, Inc., USA)

- Potassium Chloride, granular (KCl) (Mallinckrodt Baker Inc., USA)

- EDTA 0.5 M solution (Quality Biological Inc., USA)

- Calcium Chloride ($CaCl_2$) 2M solution (Quality Biological Inc., USA)

- Triton X-100 (Sigma-Aldrich Corp., USA)

- Sucrose 99.5% GC (Sigma-Aldrich Corp., USA)

- Hepes buffer 1 M solution (Cellgro® Mediatech, Inc, USA)

- Phosphate buffer saline (PBS) buffer pH 7.4 (KD Medical, Inc., USA)

Organic solvents

- Chloroform 99.9% GC (Fluka, Sigma-Aldrich Corp., USA)

- Decane 99.8% GC (Fluka, Sigma-Aldrich Corp., USA)

- Octane 99.7% GC (Fluka, Sigma-Aldrich Corp., USA)

- Squalane 99% (Supelco, Sigma-Aldrich Corp., USA)

- Methanol 99.8% GC (Fluka, Sigma-Aldrich Corp., USA)

- Ethyl Ether 99.9% GC (Fluka, Sigma-Aldrich Corp., USA)

Other

- α-chymotrypsin from bovine pancreas suitable for protein sequencing, salt-free, lyophilized powder (Sigma-Aldrich Corp., USA)

- Tris(2-carboxyethyl)-Phosphine Hydrochloride, TCEP HCl (Pierce)

- Dimethylformamide (Sigma-Aldrich Corp., USA)

- Sylgard® 184 (Dow Corning Corp., USA)

2.3. BIOLOGICAL SAMPLES

Newcastle Disease Virus Clone-30 strain was obtained from Intervet Laboratories S.A. (Salamanca, Spain). Newcastle Disease Virus *LaSota* strain was obtained from Charles Rivers Laboratories Inc., Massachusets, USA. The virus was grown in the allantoic cavity of 11 old day pathogen-free chick embryos (CBT Farm, Chestertown, MD). Upon infection, embryos were grown for 48 hours at 37ºC and 55% humidity. The allantoic fluid were then collected and stored at -4ºC. Virus was purified the next day.

2.4. ANALITICAL SOFTWARE

- Origin 7.0 (OriginLab Corp., USA) for data presentation and analysis

- MetaMorph (Molecular Devices Analytical Technologies, USA) for image analysis

- ImageJ NIH software for image analysis

- Maple Software (Maplesoft, Canada) for theoretical modelling

- AlphEase™ software (Alpha Innotech Corp., USA) for gel image analysis

2.5. METHODS

2.5.1. Virus and matrix protein purification

NDV of *LaSota* or *clone-30* strains was purified as described previously (Garcia-Sastre *et al.*, 1989). The virus was separated from the rest of the allantoic fluid by two hours centrifugation of ~500 mL of allantoic fluid at 12,000 rpm using angular rotor JA-14 (J2-21 centrifuge). The pellet was then soaked with 12 mL of 10mM Tris-HCl, 100mM NaCl and 1 mM of EDTA buffer at pH 7.4 (buffer 1) for 12 hours at 4ºC and the virus aggregate was resuspended by vigorous mixing. Six gradients of 10-50% (w/v) di-potassium tartrate were prepared by continuous gradient mixing of 17 mL of 10% solution and 17 mL of 50% solution of tartrate (both solutions were prepared by dissolving the appropriate amount of dipotassium tartrate in buffer 1). 2 mL of the sample containing resuspended virus were placed on top of the gradients and the purification was performed by overnight gradient centrifugation at 21,000 rpm with SW 28 rotor at 4ºC. A cushion containing the virus formed in the middle of the tartrate gradient. This cushion was carefully sucked with a sterile insulin syringe. To concentrate the purified virus the recovered sample was centrifuged for 1.5 hours at 34,800 rpm using a 50.2 Ti angular rotor (Optoma ultracentrifuge). The supernatant was discarded.

The Scheid and Choppin's purification protocol was used as a reference for M protein purification (Scheid and Choppin, 1973). Basic steps in this purification are outlined in Figure 9. To separate the lipid anchored proteins from the viral nucleocapsid, the virus pellet was resuspended into 10 mL of 1 M KCl, 10 mM Tris-HCl and 5 mM $CaCl_2$ containing buffer at pH 7.4 (buffer 2) with 2% the of detergent Triton X-100 and incubated 30 minutes at room temperature with constant agitation. After incubation, the sample was again centrifuged at 43,850 rpm during 2 hours at 4ºC using the SW 55Ti rotor. This time, the supernatant containing M, HN and F protein and viral lipids was recovered and dialyzed against 2 L of buffer 2 without KCl (with 5 changes) during 36 hours. This led to M protein precipitation and separation from the rest of the viral membrane proteins. The contents of the dialysis bag were centrifuged using the SW-28 rotor at 7,000 rpm, 30 minutes at 4ºC. The M protein pellet was dissolved in 1 mL of 20 mM Hepes, 1 mM $CaCl_2$ and 1 M KCl containing buffer at pH 7.0 (storage buffer).

NDV

↓

Solubilization with
2% of Triton X-100
and high ionic strength

↓

Centrifugation
200,000 x g

SUPERNATANT
(HN, F, M, lipids
and traces of NP)

PELLET
(nucleocapside)

↓

Dyalisis at
low ionic strength

SUPERNATANT
(HN, F and lipids)

PELLET
(M protein,
other traces?)

↓

Centrifugation
9,000 x g

SUPERNATANT
(Traces of
other membrane
proteins)

PELLET
(M protein)

↓

Resolubilization
at high ionic strength
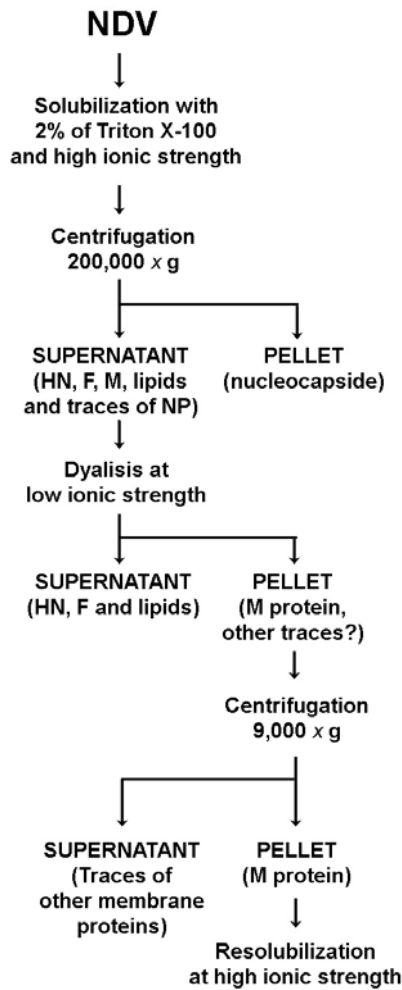
Figure 9. *Squematic representation of NDV matrix protein purification based on its aggregation at low ionic strength.*

Protein concentration was determined by the spectroscopic procedure of Markwell and co-authors (Markwell *et al.*, 1978), or with the BCA™ protein assay kit (Pierce, IL, USA), using a SpectraMax 250 microplate reader, with BSA solutions of known concentration as standards.

2.5.2. SDS-polyacrylamide gel electrophoresis, gel staining and analysis

All protein analysis by SDS-PAGE was carried out using the Novex® Pre-Cast Gel electrophoresis system from Invitrogen™. Protein or LUV-protein samples were mixed with Invitrogen's Tris-Glycine SDS sample Buffer (2x) and NuPAGE® Reducing Agent

(10x), to a final volume not larger than 35 μL. The sample vials were incubated in a water bath at 80ºC for 5 minutes to denature the protein samples. The samples were loaded into Novex® 4-20% Tris-Glycine precast gels (1.5 mm X 10 well) together with SeeBlue® Plus2 Prestained Standard (Invitrogen™). The electrophoresis was conducted at room temperature using Novex® Trys-Glycine SDS Running Buffer in the XCell SureLock™ Mini-Cell Electrophoresis System (Invitrogen™) connected to a power supply. Gels were run at a constant voltage of 120 V for 120 minutes.

After electrophoresis, gels were stained ether with SimplyBlue™ SafeStain or SYPRO® Ruby protein gel stain following the product's instructions. Stained gels were transilluminated with white or ultraviolet light for imaging of SimplyBlue™ or SYPRO® Ruby gel stains, respectively, and gels images were taken using the FluorChem® FC system. Gel background subtraction and initial gels images analysis were performed using the Alpha Ease® FC program. The data corresponding to the area under the intensity peaks of the protein bands were plotted and further analyzed using Origin 7.0 software.

2.5.3. Preparation of large unilamellar vesicles

Large unilamellar vesicles (LUVs) were prepared by an extrusion procedure (Mayer *et al.*, 1986) from the lipid mixtures listed in Table 4. Solutions of the lipid mixtures in chloroform were dried under an argon stream followed by 2 hours of incubation under high vacuum to remove traces of chloroform. Dry lipid films were then hydrated in an appropriate volume of *working buffer* (100 mM KCl, 20 mM Hepes and 0.2 mM EDTA, pH 7.4) or one of the liquid dye containing buffers (12.5 mM ANTS, 45 mM DPX, 20 mM KCl, 0.2 mM EDTA, 20 mM HEPES, pH 7.4 or 75 mg/ml 70 kDa FITC-dextran dissolved in working buffer) and dispersed by vortexing to obtain multilamellar vesicles (MLV). Lipid hydration and equal transmembrane solute distribution were promoted by 10 cycles of freezing in liquid nitrogen and thawing of the MLV dispersion. Then, the MLV dispersion was loaded into the extruder (Figure 10) preassembled with a drain disc and a polycarbonate 0.1 micron size filter. Following introduction of the sample, the extruder was pressurized with nitrogen gas and the extruded sample was recovered from

the outlet tubing. The extrusion process was repeated for a total of 10 passes. Un-encapsulated ANTS/DPX was separated from LUVs using prepacked Sephadex™ PD-10 columns. Untrapped 70 kDa FITC-dextran was removed using a Superose™ 6 packed column at a 1 mL/min flow rate. In both cases, working buffer was used as the elution buffer. The osmolality of all solutions used was measured using a vapor pressure osmometer (Wescor 5500, Logan, UT) and equilibrated accordantly. LUV preparations that were employed in experiments showed unimodal size distributions as determined by dynamic light scattering measurements. Mean diameters of LUV preparations were estimated to be 120±30 nm.

Composition	Molar composition (% each lipid)	Final lipid concentration after extrusion (g/L)	Used in
DOPC:DOPE:Chol: Rh-DOPE	60:26:10:4	0.5	Fluorimetric studies of the LUV-M protein (or BSA) interactions
DOPC:DOPE:Chol: Rh-DOPE	60:29.8:10:0.2	0.5	Fluorimetric studies of the LUV-M protein interactions
DOPC:DOPE:Chol: BODIPY-G_{M1}	60:28:10:2	0.5	Fluorimetric/Anisotropic studies of the LUV-M protein (or BSA) interactions
DOPC:DOPE:Chol: BODIPY-G_{M1}	60:29.8:10:0.2	0.5	Fluorimetric/Anisotropic studies of the LUV-M protein interactions
DOPC:DOPE:Chol: Rh-DOPE	60:29.8:10:0.2	1	M protein-LUV co-flotation binding assay
POPC:Chol:Rh-DOPE	69.8:30:0.2	1	M protein-LUV co-flotation binding assay
POPC:Rh-DOPE	99.8:0.2	1	M protein-LUV co-flotation binding assay
POPC:DOPG:Rh-DOPE	84.8:15:0.2	1	M protein-LUV co-flotation binding assay

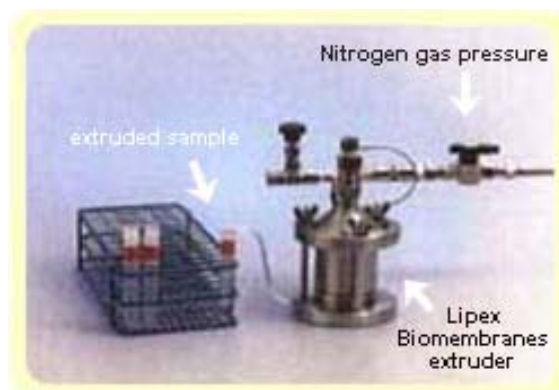**Table 4.** *LUV lipid compositions.*

Figure 10. *Thermobarrel extruder* from Lipex biomembrane Inc., USA. The MLV dispersion was loaded into the extruder preassembled with a drain disc and a polycarbonate 0.1 micron size filter. Following introduction of the sample, the extruder was pressurized with nitrogen gas and the extruded sample was recovered form the outlet tubing.

2.5.4. Analysis of matrix protein binding to large unilamellar vesicles

The amount of LUV in the LUV dispersion was normalized to the total fluorescence signal of Rh-DOPE (incorporated into LUV membrane composition) after infinite dilution with 0.1% Triton X-100. M protein (5 μM) was incubated for 5 min with LUVs of different lipid compositions or at different protein/lipid ratios. The protein bound to LUVs was separated from the unbound protein fraction using the Ficoll™ gradient flotation method (Fraley *et al.*, 1980). A non-continuous Ficoll™ gradient was prepared in polycarbonate centrifuge tubes (Figure 11). The lower layer of the gradient contained pre-incubated LUV-protein sample that was mixed with 50% Ficoll™ (w/v) dissolved in the working buffer. The final Ficoll™ concentration of the first gradient layer was 20%. The following layer contained 10% Ficoll™ dissolved in working buffer. The last layer had working buffer without Ficoll™. The gradient was centrifuged using a swinging bucket rotor (SW 55Ti) at 4ºC and 45,000 rpm for 30 minutes. Following centrifugation, the bound fraction of M was recovered together with the rhodamine labeled band of LUVs floating in the buffer-10% Ficoll layer boundary. The samples were than re-normalized against the rhodamine fluorescence signal and diluted to have the same rhodamine intensity (directly proportional to the LUV concentration). Normalized

samples were analyzed using SDS-PAGE. After electrophoresis, gels were stained with SYPRO® Ruby protein gel stain and scanned with FluorChem FC Imaging System.
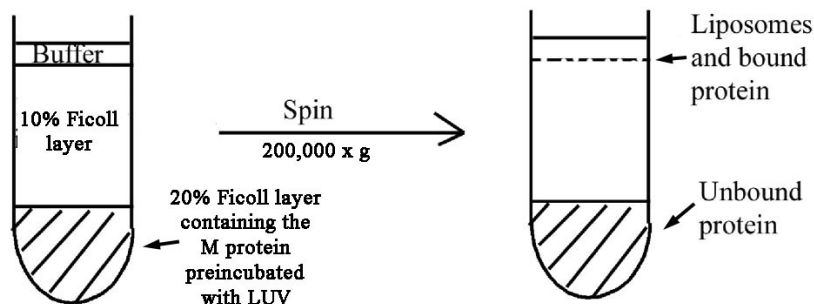

Figure 11. *M protein-LUV co-flotation gradient centrifugation assay.* A non-continuous Ficoll® gradient was prepared in a polycarbonate centrifuge tube. The lower layer of the gradient contained pre-incubated LUV-M protein sample and 20% (w/v) Ficoll® dissolved in working buffer. The following layer contained 10% Ficoll in buffer and the last layer had only working buffer. The gradient was centrifuged using a swinging bucket rotor during 30 minutes. Following centrifugation, the bound fraction of M was recuperated in the buffer-10% Ficoll layers boundary.

2.5.5. Matrix protein interaction with large unilamellar vesicles: fluorescence measurements

Leakage of ANTS or FITC-dextran and changes in fluorescence intensity of Rh-DOPE or BODIPY-G_{M1} (in quenched or non-quenched concentration) after addition of the protein sample (M protein, BSA or M protein digested 5 minutes with α-chymotrypsin (1:5 molar %)) to LUVs were determined at ambient temperature and under constant stirring by spectrofluorimetric measurements using a luminescence spectrometer. The normalized fluorescence intensity F_N was recalculated from the integral LUV fluorescence intensity as follows:

$$F_N = \frac{F - F_i}{F_f - F_i} \times 100 \qquad (3)$$

where F_i corresponds to the fluorescence intensity before the protein addition and F_f to the fluorescence intensity after complete disruption of LUV (infinite dilution of the fluorophores) by detergent (0.1% of Triton X-100). The excitation/emission wavelengths for use different fluorophores were as follows: 380/520 nm for ANTS/DPX, 550/590 nm

41

for Rh-DOPE, 505/525 nm for BODIPY-G_{M1}, and 490/520 nm for FITC-dextran. Data analysis was performed using Origin 7.0 software.

2.5.6. Preparation of giant unilamellar vesicles

The lipid mixtures used for GUV preparation are listed in Table 5. Giant unilamellar vesicles were prepared using a slight modification of the electroformation protocol (Angelova and Dimitrov, 1988). When the lipid mixture contained the charged lipid DOPG, the mixture was dissolved in chloroform:methanol:ethyl ether (4:1:5 volume ratio), to a final concentration 0.1 g/L (total lipid/solvent). In all other cases, the mixtures were dissolved in chloroform:methanol (9:1 volume ratio), to a final concentration 0.1 g/L . Two drops of 1 μL of the lipid solution were deposited on two platinum electrodes. The electrodes were dried under vacuum for at least 1 hour or overnight and then assembled on a microscopy dish with a 0.17 mm thick cover glass bottom. The dish was mounted on a stage of an inverted microscope and electrodes were then connected to the voltage generator, which applied a sinewave of 10 Hz frequency. The initial amplitude of the sinewave was 0.2 V. Right after the voltage application a buffer containing 20 mM Hepes and approximately 200 mM sucrose at pH 7.4 (osmotically equilibrated with working buffer) was added to cover the electrodes. During the following 15 minutes, the sinewave amplitude was gradually increased from 0.2 to 1.0 V. Electroformation times varied from 15 minutes to 1 hour for different lipid compositions of the GUV. After GUVs became visible on the electrode by microscopic observation, the voltage was lowered to 0.2V and then turned off completely. GUVs were either detached from the electrodes (by lowering the frequency to 0.1 Hz before lowering of the voltage) and transferred into the working buffer or left on the electrode and perfused with the working buffer.

Composition	Molar composition (% each lipid)	0.1 g/L final lipid concentration in solvent:	Used in
DOPC:DOPE:Chol: Rh-DOPE	48:43:4:5	Chloroform:methanol 9:1	GUV patching experiment and attached GUV observations
DOPC:DOPE:Chol	48:47:5	Chloroform:methanol 9:1	Effect of Cy3 labeled M protein on GUVs
POPC:Chol:Rh-DOPE	90:5:5	Chloroform:methanol 9:1	Comparison of M protein activity on different compositions
POPC:Rh-DOPE	95:5	Chloroform:methanol 9:1	Comparison of M protein activity on different compositions
POPC:DOPG:Rh-DOPE	80:15:5	Chloroform:methanol:ethyl ether 4:1:5	Comparison of M protein activity on different compositions

Table 5. *GUV lipid composition.*

2.5.7. Fluorescence microscopy observations of the interaction of matrix protein with giant unilamellar vesicles

Visualization of GUVs attached to the electrode was performed on an inverted microscope (Axiovert 200; Carl Zeiss, Inc.) using a 40x, 0.75 NA objective (ACHROPLAN; Carl Zeiss, Inc.). GUVs detached from the electrode were settled on the bottom of a 0.17mm-thin glass dish (diameter 35 mm) pretreated with 1 g/L BSA for 1 min and thoroughly washed with the working buffer to reduce GUV shrinking on the glass. The interaction of M protein with GUVs detached from the electrode was recorded using Axiovert 200 or Olympus IX-70 inverted microscopes both equipped with 150x, 1.45 NA objectives (Olympus). The images were digitized using a CoolSNAP EZ (Photometrics) or an intensified charge-coupled device camera (VE1000SIT; Dage-MTI) using IPLab (BioVision) or Metamorph Flashbus (MDS Analytical Technologies) acquisition software, respectively. The pipettes for M protein application were obtained by pulling a 1.5 mm capillary borosilicate glass with a micropipette puller. The pipette was back-filled with M protein solution using a 1 mL syringe equipped with MicroFil™ (WPI, Inc). GUV fluorescence intensity analysis was performed with MetaMorph software and data was plotted using Origin 7.0 program.

2.5.8. Cy3 maleimide staining of matrix protein

The staining of matrix protein was performed using Cy3 maleimide mono-reactive dye from Amersham Bioscience following the protocol recommended for the labelling of IgG antibody. Briefly, the protein was diluted to 1 g/L using degassed working buffer. A 100 molar excess of TCEP was added, and, after flushing the vial with nitrogen gas, the vial was closed and mixed thoroughly. The reaction was conducted at room temperature for 10 minutes. Then 50 μL of the dye dissolved in dimethylformamide was added to the reduced protein solution. The vial was again flushed with nitrogen and mixed thoroughly. The reaction was conducted at room temperature for two hours with mixing every 30 minutes and left overnight at 4ºC. The separation of the protein from free dye was done using a pre-packed HiTrap™ desalting column (GE Healthcare) attached to the peristaltic pump and a fraction collector. The dye/protein ratio of the protein eluted from the column was estimated by absorbance measurements with a Bio-Mini DNA/RNA/Protein analyzer (Shimadzu), using extinction coefficients of 150,000 $M^{-1}cm^{-1}$ at 552 nm for Cy3 and 30,000 $M^{-1}cm^{-1}$ at 280 nm for matrix protein, and taking into account that the dye contributes to the absorbance at 280 nm which is about 8% of its absorbance at 552 nm. The dye/protein ratio was estimated as:

$$\frac{Cy3\_dye}{M\_protein} = \frac{A_{552}/150,000}{[A_{280} - (0.08 \times A_{552})]/170,000} \approx 4 \qquad (4)$$

While this measurement indicates that about 4 dye molecules are conjugated to each protein, the expected fluorescence signal is hard to estimate due to the possibility of quenching of the dye fluorophores located on the protein.

2.5.9. Detection of vesicle budding/fission by admittance measurements

Planar bilayer lipid membranes (BLM) were formed by the Mueller-Rudin technique (Mueller and Rudin, 1967) from a lipid solution in squalane. The lipid mixture was prepared from stock solutions of DOPC:DOPE (2:1 molar %) and 20 molar % cholesterol in chloroform. The chloroform was evaporated under argon (30 min/60μL

volume) and squalane or a decane:octane mixture (1:1 v/v) were added to reach a final concentration of 20 mg of lipids per 1 mL of solvent.

BLM was formed on an aperture of a horizontal Teflon film (thickness 40 μm), separating upper and lower compartment of a special chamber (Figure 12). Apertures of 100–200 μm in diameter were punctured by an injection needle. The aperture was pretreated with 5 μL of the lipid solution in decane/octane (1:1) and left in vacuum for ~30 minutes to let the solvents evaporate. Then the chamber was filled with electrolyte (working buffer) and mounted on the stage of an inverted microscope (Olympus IX-70); the orifice was visualized by phase-contrast microscopy using a 40X objective. BLM was formed up by the "painting" technique: a small amount of the lipid solutions in squalane was picked by a sable brush and deposited across the orifice so that a thick film covering the orifice was formed. If necessary, the excess of the solution was removed by a clean brush. The film then thinned spontaneously as seen by the formation of a clean round area in the phase-contrast image and an increase in the electrical capacitance of the film. To monitor electrical parameters of the film, Ag/AgCl pellet electrodes were immersed into both compartments of the chamber. The upper electrode was inside a standard patch-clamp pipette (see below), while the lower electrode was immersed directly into the lower compartment (Figure 12A). An EPC 7 patch clamp amplifier (HEKA) and PC-44 acquisition board with on-board software lock-in (Bronew software (Ratinov *et al.*, 1998), available upon request) were used to apply voltage and record electrical current from the BLM. The specific capacitance of thin films was estimated to be 0.9–1.0 μF/cm^2, corresponding well to the values characteristic for bimolecular lipid films published elsewhere (Melikov *et al.*, 2001).

BLM was patch-clamped by a pipette (Lollike and Lindau, 1999) containing M protein (0.2 μM, estimated ~0.05 molar protein/lipid ratio or 5 μM). 1–3 MOhm Sylgard-coated borosilicate glass pipettes filled with working buffer were used. The pipettes were brought to the BLM using precise piezo micromanipulators. After formation of a tight giga-seal (Neher and Sakmann, 1992) contact between the pipette and BLM (Figure 12B), a 5000 Hz, 100 mV sine-wave potential superimposed with a 20 mV constant holding potential V_{hold} was applied. The resulting current was decomposed by the Bronew software onto 3 components (direct current (DC) and 2 components of alternating current

(AC), sin phase and 90°-shifted with respect to the applied voltage; the phase correction was performed by dithering the C-fast compensation circuit of the EPC-7 amplifier as described elsewhere (Neher and Sakmann, 1992)). Data were stored on the hard drive of a PC computer and analyzed off-line.
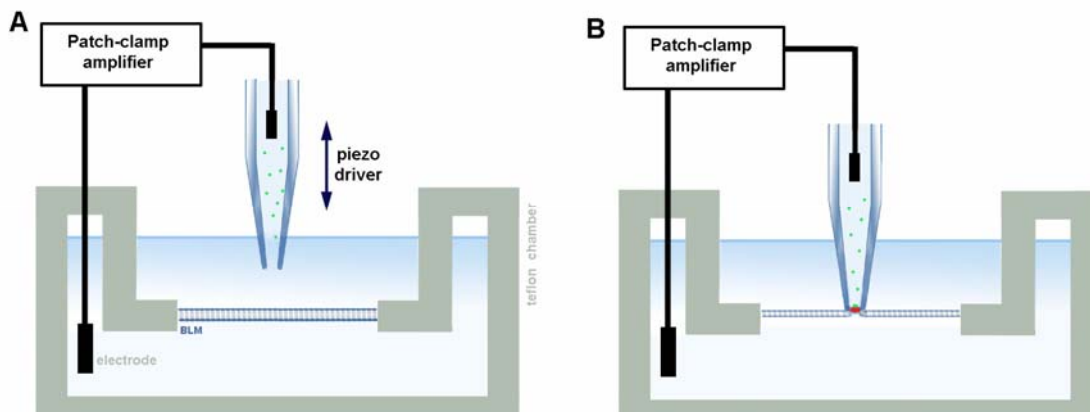

Figure 12. *Experimental setup for electrical admittance measurements.* **A.** BLM is "painted" on a hole in the Teflon film partition. To monitor electrical parameters of the membrane film, Ag/AgCl pellet electrode is immersed into the lower compartment of a teflon chamber and the upper electrode is inserted inside a standard patch-clamp pipette containing the protein solution. **B.** After the pipette enters in contact with the membrane by its piezo manipulation, a giga-seal is established between the patch area (represented in red) and the pipette tip, allowing for patch capacitance monitoring.

Generally, changes in the direct current (DC) indicate formation of conductive pathways (such as channels or pores) allowing for direct translocation of ions across the BLM patch inside the pipette. Changes in the amplitudes of the two components of the alternate current (AC) are proportional to the real (ΔRe) and imaginary (ΔIm) parts of the electrical admittance of the patch (Frolov *et al.*, 2003). Besides formation of pores and channels, these changes also report total electrical capacitance and geometry of the patch. The capacitance of the patch may be further analyzed in terms of the bud area as:

$$C_{bud} = A_{bud} * C_0 \qquad (5)$$

where C_{bud} is the capacitance of the bud at the maximum value of ΔIm, A_{bud} is the total area of the bud and C_0 is the specific capacitance of the membrane.

A flat unperturbed membrane patch (e.g. as in control experiments where no proteins was added to the patch-pipette) is well described by a single capacitor (see equivalent

circuit in Figure 23b) and its DC conductance (G_{DC}) is negligible. Thus, at the reference state, the DC signal through the patch is at a background (zero) level ($G_{dc}=I_{dc}/V_{hold}$), and so is the real part of the admittance (Re). The imaginary part of the admittance, ΔIm, is proportional to the total electrical capacitance of the patch: Im=αC_{patch}, where α is the proportionality factor. Thus, the Im channel is calibrated using the C_{fast} compensation circuit of the EPC-7 amplifier, so that α is found and further used for the analysis of admittance changes. To increase the dynamic range and signal-to-noise ratio of the measurements, the initial capacitance of the patch is then compensated, so that only changes in amplitudes of Re and Im components of the AC current (ΔRe and ΔIm) are recorded.

Recordings were started after the calibration and compensation procedures are finished: typically ~ 1min after establishment of the giga-seal contact between the patch-pipette and BLM.

ΔRe and ΔIm were analyzed off-line (assuming the formation of a bud with capacitance C_{bud} connected to the reservoir membrane by a neck with conductance G_n) using the following formulae resulting from the equivalent circuit analysis:

$$\Delta\,\mathrm{Re} = \frac{G_n}{(\dfrac{G_n}{\omega * C_{bud}})^2 + 1}\,; \qquad (6)$$

$$\Delta\,\mathrm{Im} = \frac{\omega * C_{bud}}{(\dfrac{\omega * C_{bud}}{G_n})^2 + 1}\,; \qquad (7)$$

where $\omega=2\pi f$, and f is the sine wave frequency. In general, the capacitance of the bud membrane C_{bud} and G_n were calculated offline according to the formulae (easily obtained from (1) and (2)):

$$C_{bud} = \frac{\Delta\,\mathrm{Re}^2 + \Delta\,\mathrm{Im}^2}{\omega\Delta\,\mathrm{Im}} \qquad (8)$$

$$G_n = \frac{\Delta\,\mathrm{Re}^2 + \Delta\,\mathrm{Im}^2}{\Delta\,\mathrm{Re}} \qquad (9)$$

2.5.10. Analysis of matrix protein condensation on lipid monolayers

The specially designed teflon chamber was used (Ford *et al.*, 2001) as shown in Figure 13. 2 μL DOPC:cholesterol (9:1 molar %, 0.1 g/L final concentration) lipid solution in methanol/chloroform (9:1) was deposited on the working buffer-air interface (the buffer volume in the chamber was about 400 μL) to form a lipid monolayer. After one hour equilibration, a carbon-coated gold EM grid was placed on top of the buffer droplet where the lipid monolayer had been formed. 0.13 μg of M protein was applied to the buffer from a side opening using a hamilton syringe. After 1 hour incubation the grid was carefully removed and stained with uranyl acetate (2% solution in water) for further observations with Tecnai G2 transmission electron microscope (FEI Company) at 120 kV.
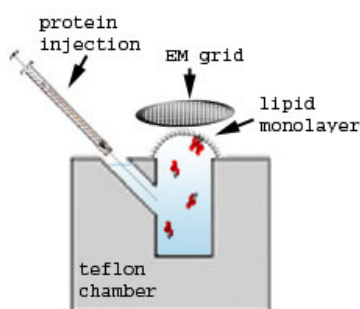
Figure 13. *Assay for M protein condensation on lipid monolayer.* First the lipid monolayer is deposited on the buffer droplet. After the monolayer has stabilized, EM grid is applied on top. Protein is injected form the side orifice using a Hamilton syringe. After a period of incubation, the grid is removed and negatively stained before the TEM analysis.

2.5.11. Preparation of lipid monolayers

MicroTrough S (Kibron Inc., Finland) apparatus was used to study the lipid, protein or lipid-protein monolayer properties (Figure 14). For preparation of a lipid monolayer, 10 μL of a hexane solution of DOPC:Cholesterol (9:1 molar %, 0.5 g/l) was spread on the surface of the working buffer. After 20 minutes, the monolayer was slowly compressed and the corresponding surface pressure-area isotherm was recorded using

FilmWare 2.41 Kibron software. The same procedure was performed to study the M protein formed films, where 10 μL of M protein diluted in the working buffer (final concentration 0.6 g/L) was deposited on the buffer-air interface. In the case of M protein interaction with the lipid monolayer, the lipid monolayer was first pre-formed and compressed to ~ 2 mN/m. MicroTrough S system allowed displacing the barriers so that the compressed lipid monolayer was on one side of the trough and the protein could be applied from the other side. After the pre-compression, the lipid monolayer was slowly moved toward the zone where the protein was applied. The resulting protein-lipid monolayer was stabilized during 20 minutes and then compressed to obtain the surface pressure-area isotherm, which was then plotted and analyzed using Origin 7.0 software.
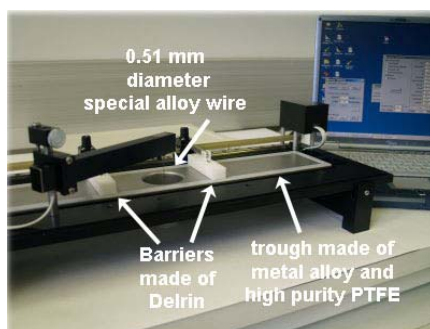
Figure 14. *Photograph of MicroTroughX apparatus* (Kibron Inc.). While the barriers are in their extreme positions, the trough is filled with the subphase (working buffer) and the desired film is applied on top of the subphase. After the monolayer stabilization, the barriers are compressed and the surface pressure-area isotherm is measured by Wilhelmy method as the force due to surface tension on the suspended wire is measured by a microbalance.

There are three principal means of acquiring knowledge available to us: observation of nature, reflection, and experimentation. Observation collects facts; reflection combines them; experimentation verifies the result of that combination. Our observation of nature must be diligent, our reflection profound, and our experiments exact.

Denis Diderot

III. RESULTS AND DISCUSSION

3.1. Purification of matrix protein from Newcastle Disease Virus: effect of calcium

Various viral matrix proteins are known for their ability to self-assemble into ordered structures in low salt solutions. The speed and efficiency of such aggregations are usually determined by ionic strength and protein concentration (McCreedy *et al.*, 1990). This sensitivity has been routinely used to separate matrix protein from the rest of the viral proteins: M protein appears mostly as a monomer at high ionic strength, but aggregates slowly and irreversibly at physiological ionic strength (Sagrera *et al.*, 1998). Accordingly, the use of high ionic strength (>1M) solution during purification is critical for disassembly of the interior of NDV. However, some experimental observations indicate that M protein interaction with NP protein is not totally disrupted during the purification procedure based on salt concentration changes, and that the aggregation of M protein may be in part due to the formation of this M-NP complexes. At the initial state of this work it was found that calcium at milimolar concentration allows a better separation of M protein from the NP complex, presumably through disruption of some electrostatic interactions (Figure 15A).
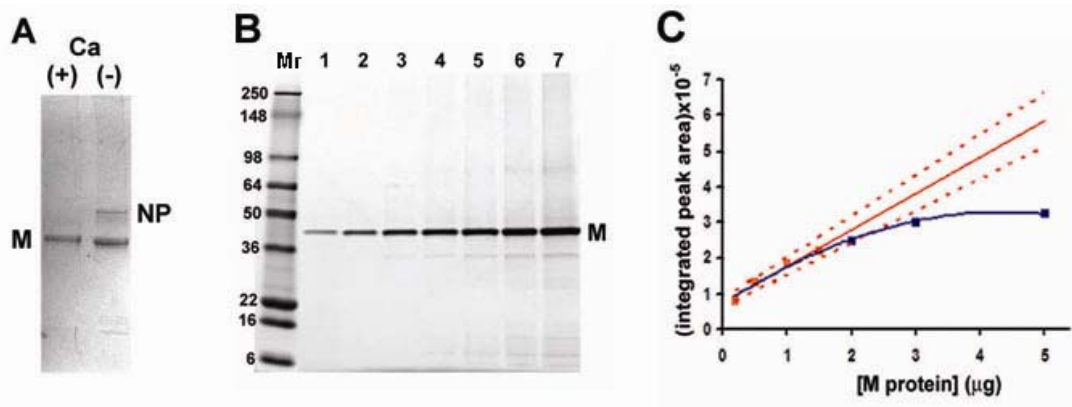

Figure 15. *M protein purification and analysis of the protein purity by SDS-PAGE.* **A.** Comparison of the final products of the M protein purification procedure conducted with (5 and 1 mM Ca^{++}, right lane) and without calcium (left lane). The addition of millimolar calcium to the buffers during the protein purification augmented disruption of the M-NP protein complex. **B.** Analysis of the purity of M protein purified in the presence of Ca^{++}. The first lane of the gel shows molecular weight standards; 0.2, 0.5, 1, 1.5, 2, 3 and 5 µg of M protein were loaded into lanes 2 to 8, respectively. The gel was stained with SimplyBlue[TM] (Invitrogen), scanned, and the densitometry analysis of the protein bands in each lane was performed in accordance with the procedure developed earlier (Materials and Methods). **C.** The graph shows the dependence of the area under the peak attributed to the M protein band (without impurities) on the total amount of M protein loaded in the lane; red line is the linear extrapolation calculated on the first four points corresponding to non-saturated M protein loads. The confidence intervals (95%) of this extrapolation are indicated with the red dotted lines.

This modified protocol allowed obtaining highly purified M protein. The protein purity was estimated from SDS-PAGE gel (Figure 15C) according to a procedure based on analysis of the areas under the intensity peaks (corresponding to protein bands) (Coorssen *et al.*, 2002). The intensity curves in Table 6 correspond to the individual lanes in the gel showed in Figure 15B. Graphic representation of the peak area values versus the amount of protein loaded in the lane demonstrates a non-linear dependence (Figure 15C). However, the first four point of the curve can be linearly fitted (red line in Figure 15C, r=0.985). Extrapolating the line defined by the fitting parameters over the last points of the curve, the expected peak intensity for the 5 µg of pure protein is obtained. Then, the purity of the M protein in the sample can be estimated as:

$$ Purity\% = \frac{A_{Pure\_protein} - A_{all\_impurities}}{A_{Pure\_protein}} \times 100 \qquad (10) $$

where *A* denotes the area under the intensity peaks. A purity of 94±2% (at 95% confidence interval (Coorssen *et al.*, 2002)) was obtained.

GEL LINE #:	1	2	3	4	5	6	7
µg OF M PROTEIN LOADED:	0.2	0.5	1	1.5	2	3	5

	1	2	3	4	5	6	7
Peak 1:	82851	134203	183276	220081	246137	301376	323359
Peak 2:	-	-	-	1516	1944	2632	27322
Peak 3:	-	-	-	-	-	1222	1853
Peak 4:	-	-	-	-	-	-	1344
Peak 5:	-	-	-	-	-	-	4779
Total area of all peaks minus M protein peak contribution	0	0	0	1516	1944	3854	35298

Table 6. *Analysis of intensity curves plotted for the individual lanes in the gel showed in figure 15C.*

3.2. Matrix protein associates with and deforms large unilamellar vesicles

The characterization of M protein binding to large unilamellar vesicles (LUV) of different lipid compositions was performed to define the membrane composition preferences of M protein from NDV *LaSota* strain.

The co-flotation assay (see Material and Methods) was chosen to monitor irreversible binding of the protein to LUVs. This assay showed tight binding of M protein that is dependent on the lipid composition of the membrane and on the protein concentration (Figure 16A and B, respectively). In addition, M protein showed a higher affinity to LUVs whose composition contained cholesterol, or PE and cholesterol (as can be observed in Figure 16A). Presence of negatively charged lipids in the LUV membrane composition did not improve the binding of the protein, thus indicating the hydrophobic character of M protein-membrane association apparently is mediated by the protein insertion into the lipid bilayer. This result is in a good agreement with the previously reported study of M protein from another NDV strain (Australia-Victoria), where the interaction of the protein with multilamellar liposomes was also shown to be non-electrostatic (Faaberg and Peeples, 1988). The membrane composition to which the protein showed the highest affinity was chosen to perform all subsequent protein-membrane interaction studies. If not indicated otherwise, the default lipid composition for the different lipid systems used is DOPC:DOPE:Cholesterol in variable molar ratios.

The vesicle stability upon M protein adsorption was explored using LUVs loaded with aqueous fluorescent markers, either small (ANTS/DPX) or large (70 kDa FITC-dextran). Starting at ~0.01 protein/lipid ratio, release of both markers was seen with slower kinetics for the larger marker (Figure 16C, blue and green squares). The possibility that the observed effects of the protein were caused by some artifact present in the protein solution (for example, the detergent triton that was used during the protein purification) was checked by α-chymotrypsin proteolytic treatment of the protein (Figure 16D). After this treatment, the efficiency of content release from LUV after protein addition was greatly impaired (Figure 16C, blue and green triangles).
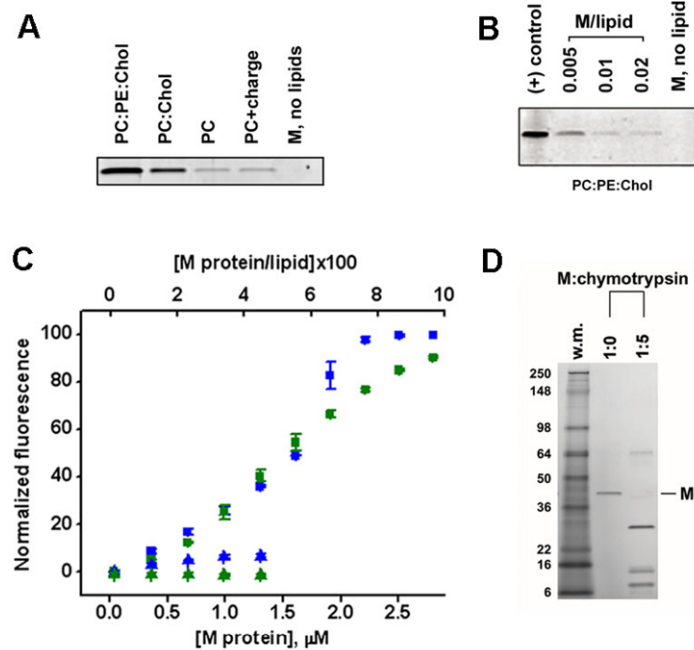
Figure 16. *Characterization of M protein interaction with large unilamellar vesicles.* **A.** M protein adsorption on LUV of different lipid composition (0.005 protein/lipid ratio) measured by gradient flotation technique; protein was loaded in the same concentration in all bands; control fraction (M, no lipids) was taken at the same level as the liposome fraction. **B.** M protein adsorption on PC:PE:Chol LUV at different protein/lipid ratio measured by liposome co-flotation assay (see Material and Methods); the same protein concentration for all bands was loaded; control fraction (M, no lipids) was taken at the same level as the liposome fraction; positive control shows known M protein sample loaded in the band. **C.** Sequential additions of 0.3 μM of M protein induce release of LUV entrapped ANTS/DPX (blue squares) or 70-kDa FITC conjugated dextrans (green squares) seen as changes of normalized fluorescence intensity (Material and Methods). Addition of the same amount of the protein cleaved by α-chimotrypsin caused minor release of ANTS/DPX and dextrans (blue and green triangles); bars show SD. **D.** Proteolitic treatment of M protein. The protein (5 mM) was incubated for 5 minutes at room temperature with the amount of α-chimotrypsin indicated in the gel picture; the reaction was stopped by addition of SDS sample buffer and the resulting material was analyzed by SDS polyacrylamide electrophoresis. The first lane shows molecular weight standards.

Release efficiencies were comparable for both high and low molecular weight markers for the same amount of the protein added, thus indicating vesicle bursting. In corroboration of this notion, the extent of content release grew almost linearly, as it does in experiments on the osmotic rupturing of LUV (Mui *et al.*, 1993) (Figure 17A). Additionally, formation of pores by M proteins was excluded by electrophysiological measurements (see below). Consequently, the most likely cause of LUV bursting was membrane deformation. M protein induced LUV content release at relatively high surface coverage (estimated as one M protein per ~8 lipids in the outer monolayer). At this concentration, M proteins could self-assemble on the liposome membrane and bend it

inward (Figure 17B) as VSV matrix proteins do (Solon *et al.*, 2005). Most deformations of a quasispherical LUV increase its surface/volume ratio, thus attempting to stretch the liposome membrane. Accordingly, the inward bending would tend to stretch the LUV membrane (Figure 17C; $(S_1+S_2)>S$) leading to its rupture if the M protein cap covers enough LUV area (10 % of the LUV area should be covered by the protein (see appendix I), comparable with estimates from experimental data).
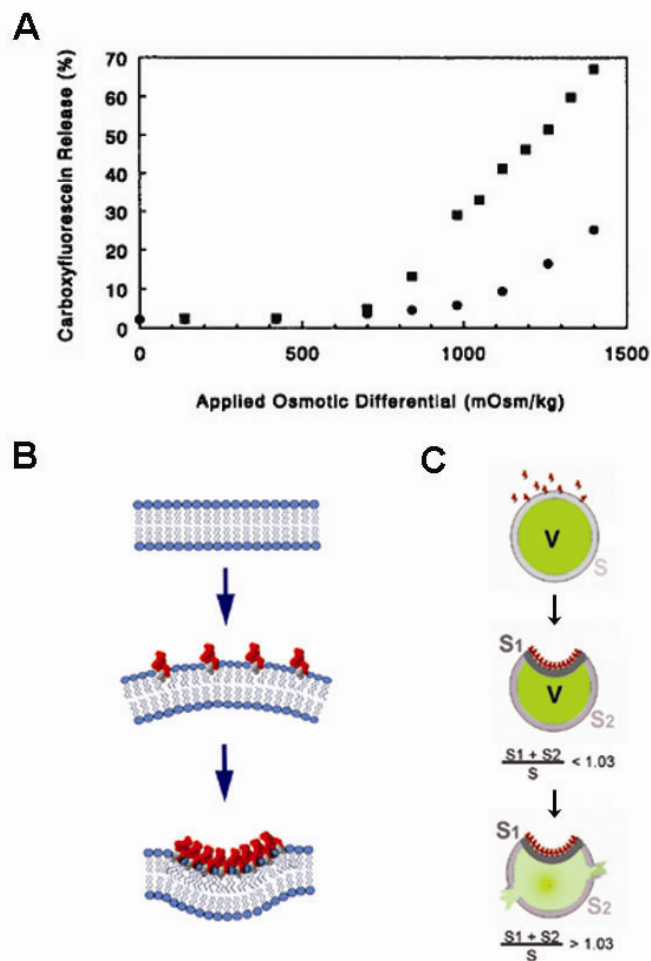
Figure 17. *Rupture of large unilamellar vesicles by M protein induced membrane stress.* **A.** Osmotic pressure induces carboxifluorescein release from LUV (Mui *et al.*, 1993). **B.** Schematic representation of M protein oligomerization causing invagination of the membrane of spherical LUV. It is assumed that M proteins bring negative curvature characteristic for the NDV membrane ($\sim$ -0.3 μm^{-1}), while the LUV radius is assumed to be 0.1 μm. **C.** M protein-induced invaginations result in an increase of the LUV membrane area, if the LUV volume (V) is maintained constant (see Appendix I). The membrane area can increase only in $\sim$3% before rupturing[27]. In appendix I it is discussed how 3% of LUV area increase corresponds to $\sim$10% area coverage by the M proteins.

Until the protein/lipid ratio of ~0.01, no release of LUV contents was detected (Figure 16C). Yet, M protein bound to LUVs even at lower protein to lipid ratios (Figure 16B), indicating that a critical amount of M protein on a liposome surface was needed to initiate the content release. The binding threshold before the effect of the protein on LUV may be an indication of the two-dimensional self-assembly of M protein on the membrane surface. These results, together with the M protein capacity to aggregate in solution (upon lowering of ionic strength (Sagrera *et al.*, 1998)) and its tight lining of the virus membrane (Faaberg and Peeples, 1988), are apparently in agreement with the hypothesis of M protein self-assembly on the membrane surface into a domain, likely stabilized by electrostatic interactions.

To further investigate the origin of M protein-membrane interaction, LUVs were loaded with rhodamine-DOPE or another membrane probe, BODIPY-G_{M1} in self-quenched concentration. Both types of membrane markers showed similar fluorescence increase (dequenching) upon M protein addition. In contrast, addition of another membrane active protein, BSA, to the same LUVs resulted in a slight decrease of the fluorescence (Figure 18A). M protein caused no effect on the fluorescence of LUVs containing non-quenched dyes (Figure 18A). Though the exact mechanism of dequenching of membrane fluorescence by M protein had not been resolved, similar behavior of different fluorophores precluded specific interactions between the fluorophore and the protein. More likely, the fluorescence increase corresponds to general constraints of lipid mobility known to be imposed by membrane-associating M proteins (Neitchev and Dumanova, 1992). Confirming this hypothesis, the increase of steady-state anisotropy of BODIPY-G_{M1} fluorescence (reporting the probe mobility (Marushchak *et al.*, 2006)) upon M protein addition was detected for the self-quenched and non-quenched dye (Figure 18B). Again, a likely explanation of this phenomenon is protein self-assembly into a domain on the lipid membrane surface.

To summarize, experiments with LUV resulted in initial characterization of the M protein-lipid interactions (including quantification of binding) and suggested formation of membrane domains by M proteins. To visualize M protein activity and check the validity of the domain hypothesis giant unilamellar vesicles were used.
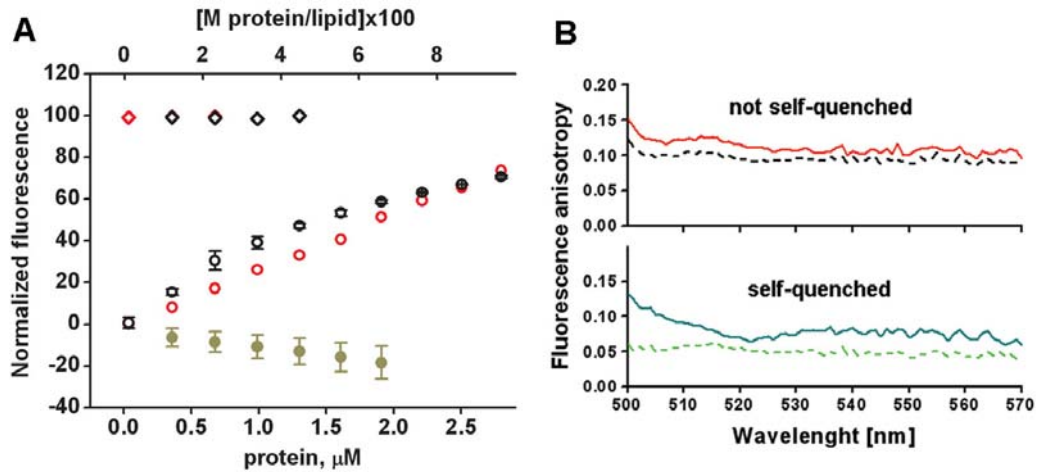
Figure 18. *M protein adsorption induces changes in fluorescence of lipid probes incorporated into LUV.*
A. Sequential additions of 0.3 μM of M protein or BSA to LUV cause dequenching of Rh-DOPE or BODIPY-G_{M1} fluorescence (red and black circles); no changes were detected for non-quenched dyes (red and black open diamonds) or when BSA was added (dark yellow circles). **B.** Measurements of the anisotropy of the BODIPY-G_{M1} fluorescence. Anisotropy of the fluorescence of BODIPY-G_{M1} incorporated in LUV was measured as described earlier (see Material and Methods). LUV contained either 2 molar % (self-quenched) or 0.2 molar% (non-selfquenched) of the probe. The anisotropy spectra were collected before (dark and light green) and 10 minutes after (red and dark green) the M protein addition in final concentration of 2 μM. For both, quenched and non-quenched dye, the anisotropy curve raised indicating decreased mobility of the fluorophores.

3.3. Matrix protein induces budding upon adsorption on giant unilamellar vesicles: fluorescence microscopy observations

Giant unilamellar vesicles (GUV) containing fluorescently labeled lipid (rhodamine-DOPE) in self-quenched concentration were used to visualize the interaction of M protein with lipid membranes by fluorescence microscopy. In the first round of experiments, a small patch of GUV membrane was isolated inside a pipette containing M protein. Shortly after establishing a stable contact between the GUV membrane and the pipette containing 2 μM M protein solution, the fluorescence intensity of the membrane patch inside the pipette increased sharply (Figure 19A, second frame expanded with false-color in Figure 19B). The following membrane rearrangements resulted in the budding of round vesicles of different diameters visible near the patch. The membrane outside the patched area provided a lipid reservoir to support this small vesicle formation from the giant mother vesicle. With retrieval of the membrane area into the internal vesicles, GUV

57

diameter decreases progressively: thus the contact with the pipette did not interfere with lipid exchange between the mother membrane and the isolated membrane patch. Finally the GUV membrane detached from the pipette and multiple vesicles were seen moving inside the GUV (Figure 19A, see also movie1 in appendix II).
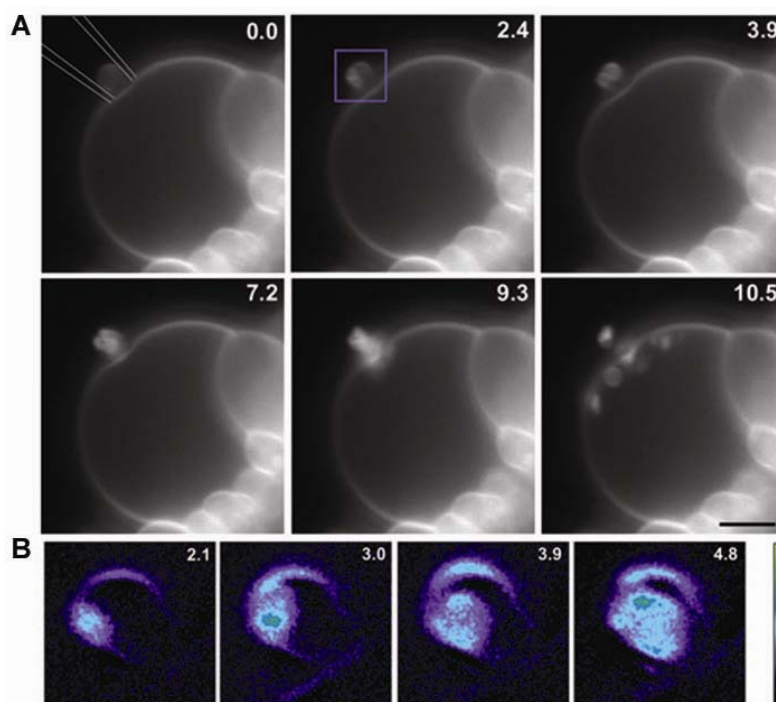

Figure 19. *Interaction of M protein with a membrane patch of the GUV isolated by a patch-pipette.* **A**. Frame sequence (time in seconds) illustrating membrane budding from a patch-pipette (approximately drawn in the first image) containing M protein (2 μM). A small part of the large GUV, attached to platinum electrode used for electroformation, was sucked into the pipette. The recording began shortly after the establishment of a stable contact between GUV and the pipette; bar 5 μm. **B.** Expanded images, showing the area marked by the blue rectangle in A, illustrating the brightening of the membrane patch upon M protein adsorption.

In a second set of experiments, the pipette containing a concentrated solution of the protein (4 μM) was placed near the GUV. The protein was applied by a pulse of positive hydrostatic pressure so that the protein concentration in the GUV vicinity increased transiently. Shortly after protein application, formation of bright spots within the original GUV contour was observed (Figure 20A, movie2 in appendix II). Appearance of the spots corresponded to a sharp increase in the average fluorescence intensity calculated in the GUV projection area (Figure 20B). These brightened areas were subsequently invaginating (Figure 20B, arrow). When only a short pulse of the M protein

was applied, the deformations gradually disappeared while the protein concentration decreased as the proteins diffused away from GUV. Finally, the GUV relaxed to its original spherical shape (movie 2 in appendix II). This shape relaxation coincided with a decrease in the fluorescence of the GUV membrane to a new steady-state level (Figure 20B, I_2). Both shape and fluorescence changes could be initiated again by application of more M protein until the GUV was completely destabilized. After each protein application the apparent size of the GUV decreased and the steady-state fluorescence of the GUV projection area increased (Figure 20B, from I_1 to I_2). Internalized membrane vesicles were clearly detected, thus justifying this fluorescence changes (Figure 20A, see also Figure 22 with different lipid composition).
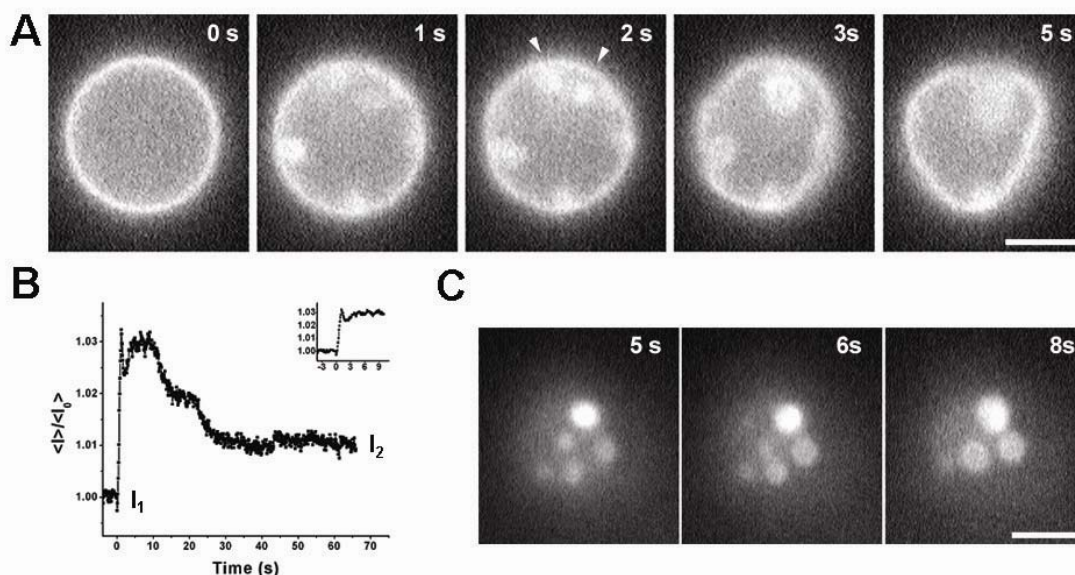
Figure 20. *Interaction of M protein with GUV: membrane domains and deformations.* **A.** Changes of membrane fluorescence followed by membrane deformations induced by a transient application of M protein (added at t=0) to a GUV made of PC:PE:Chol mixture; white arrows show joining of bright membrane domains; **B.** Analysis of fluorescence intensity changes in the time sequence from A. C. Bright spots appear and merge after M protein application to a GUV flattened on the glass surface, bars 5 μm.

In a slight variation of the previous experiment the protein was applied near a vesicle that was deflated on the cover glass (Figure 20C). Once again the emergence of bright round spots which grew by fusing together preceded the membrane budding (see movie3 in appendix II).

An attempt to label the protein on its five cysteine aminoacids using Cy3 maleimide compound was made as described in Materials and Methods section. The resulting labeled product had 4 dye molecules per protein molecule. However, while the labeled protein was able to bind uniformly to the membrane of the GUV, no self assembly into round domains was observed (Figure 21). This lack of self-assembly correlated with lack of budding activity: in none of the 10 experiments performed with the labeled protein was internal vesicle formation observed. It is likely that the labeling of some of the 5 cysteines present in the matrix protein impeded electrostatic interactions between M proteins.
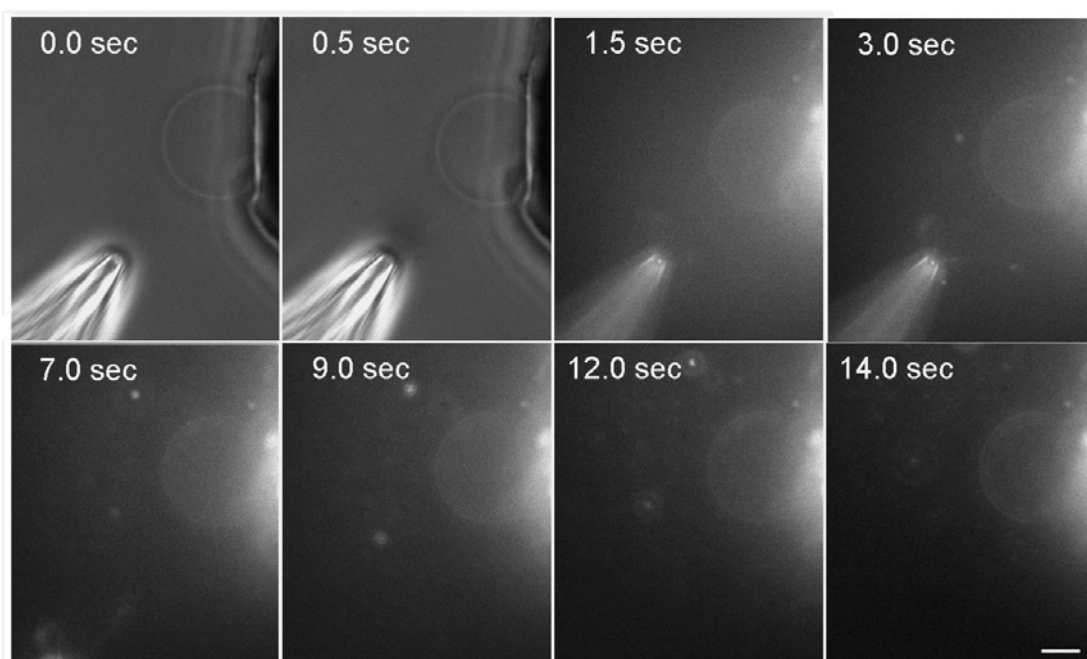
Figure 21. *Adsorption of M proteins labeled by Cy3 fluorophores on GUV membrane.* The labeled M protein (0.5 μM) was applied from a delivery pipette placed near a GUV, as seen in the first two frames showing bright-field images. Subsequent fluorescence images (time in seconds) show adsorption of labeled M proteins on the GUV. Note that no membrane deformations are visible. Upon M protein adsorption, GUV remained uniformly labeled (frame 2-6). Bar 3 μm.

Though no direct observations of the functional proteins could be made, the results of the experiments on GUV containing self-quenched rhodamine in the membrane clearly demonstrated the formation of domains that bud away from the membrane. Altogether, the experimental data obtained on LUV and GUV show that these domains are assembled by M proteins. Indeed, from LUV experiments described in the previous

60

section it can be extrapolated that dequenching of rhodamine florescence, also observed in GUV, correlates with protein adsorption on the membrane. Unidirectional membrane budding that follows the protein adsorption, directly indicates that budding domains contain M proteins imposing negative curvature – if they were "holes" (circles) of pure bilayer, then bidirectional budding would be the likely outcome. It can be also excluded that M proteins form a rigid sheet from which membrane bud tears out; multiple budding event from a patch would not be possible. The lack of budding in the absence of bright domains is indicative of protein self-assembly on membrane surface as an important step in the vesiculation progress. Finally, efficient formation of vesicles from a patch of GUV membrane (Figure 19) demonstrates that the budding is a localized event rather than a consequence of bulk shape transformations of a GUV that can be caused by massive protein adsorption (Tsafrir *et al.*, 2003).

As can be observed in the Figure 22, vesicle formation was more effective when cholesterol or charged lipids were present in the GUV composition. As shown above, the binding efficiency of M protein to LUVs was not affected by the membrane charge (Figure 16A). Thus, charge lipids enhance the budding activity of already bound M proteins. Cholesterol, on the other hand, stimulates both adsorption and budding activity of M protein. Notably, with the addition of 30 molar % of cholesterol, which doubles the bending rigidity of the GUV membrane (Henriksen *et al.*, 2004), the budding efficiency of M protein was not diminished but rather augmented (Figure 22). This finding demonstrates that cholesterol, an abundant component in the NDV membrane, can actively participate in virus budding (Laliberte *et al.*, 2007). Interestingly, the presence of PE also increased protein adsorption and supported effective membrane budding (see Figure16A and Figure 22), likely through its intrinsic negative curvature.
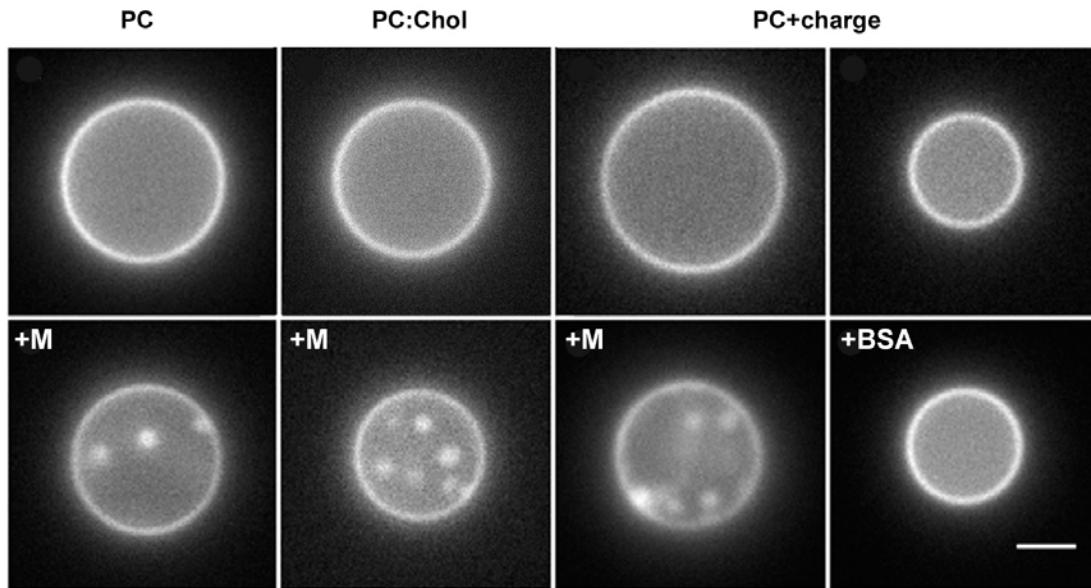
Figure 22. *Effect of M protein and BSA adsorption on the morphology of the GUVs with different lipid compositions.* M protein (4 μM) or BSA (4 μM) was applied from a delivery pipette. Images were taken before (upper row) and ~2 minutes after (lower row) the protein application; representative images of 3 independent experiments are shown; bar 2 μm.

Overall, vesicle formation and changes in membrane fluorescence were detected with 4 different batches of M protein (18 experiments total). No comparable changes were observed on GUVs perfused with buffer containing no protein or 4 μM BSA (Figure 22). The spatial resolution of fluorescence microscopy, limited to ~micron size objects, did not allow for detection of smaller vesiculation events comparable with those expected for a NDV particle (100-300 nm). However, these experiments show that through interactions with lipid bilayer, M protein implements the genetically encoded information required to create the closed spherical membrane particles; thus virus geometry resides with its M protein.

To characterize smaller budding events induced by M proteins on a lipid bilayer surface, measurements of electrical admittance on a planar BLM were performed.

3.4. Budding activity of matrix protein monitored by admittance measurements

As in experiments with GUV, a small patch of a BLM was isolated inside a patch-pipette containing M protein solution. Changes in the electrical admittance of the patch were monitored as described in Materials and Methods.

To proceed with further analysis of experimental data it is instructive to review the expected changes in the equivalent electrical circuit of the membrane patch during a budding event (Figure 23). Assuming that M protein mediates formation of spherical particles from the membrane patch, as it does on a plasma membrane or in GUV experiments described above, the growing bud would retrieve the "initial" area of the patch (Figure 23A, yellow). Consequently, the total membrane area localized within the patch pipette would increase as additional area is retrieved from reservoir (blue in Figure 23B). The apparent electrical capacitance of the patch, proportional to the total membrane area inside the pipette, will increase as well. If the bud finally pinches off (as in cellular systems (Rosenboom and Lindau, 1994)), the membrane area inside the patch will decrease and the capacitance (ΔIm) will return to its initial level (Figure 23C).
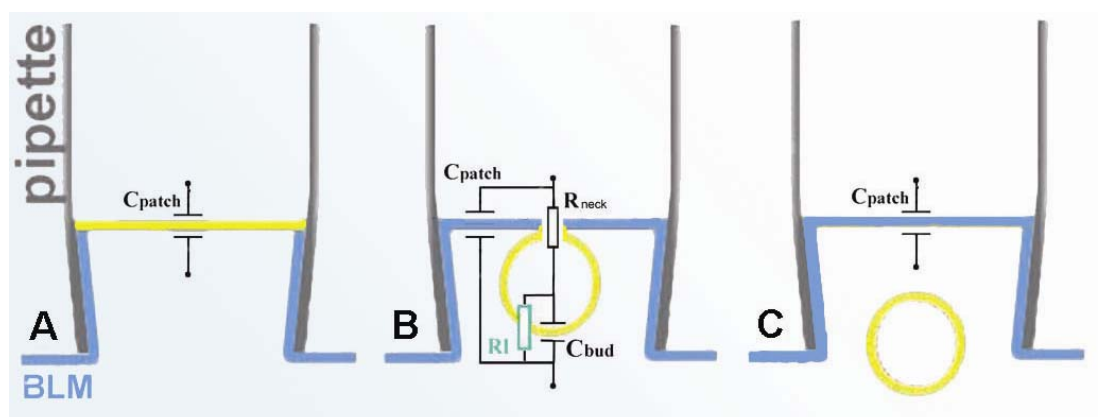

Figure 23. Changes in the equivalent electrical circuit of a membrane patch during budding of small spherical vesicles. A. A large planar BLM attached to a lipid reservoir is patch-clamped by a narrow glass pipette isolating a small membrane patch (yellow) (Melikov et al., 2001). The intact patch has very small ionic permeability and thus is characterized only by its electrical capacitance, C_{patch}. **B.** When a vesicle is derived from the patch it recruits its initial membrane (yellow) and additional membrane is retrieved from the reservoir (blue) to satisfy boundary conditions for the stable patch (it is assumed that vesicle formation does not affect the contact between the membrane and the pipette). The equivalent circuit now includes 3 additional elements: C_{bud} corresponds to the bud area; R_{neck} corresponds to the access resistance of the neck connecting the vesicle and the membrane patch at the late stage of budding; R_l corresponds to the leakiness of the vesicle membrane; all elements can be calculated from measured changes of the equivalent admittance (ΔIm and ΔRe) and DC-conductance (G_{dc}) of the membrane system within the pipette (Lollike and Lindau, 1999). **C.** After the vesicle pinches off, the equivalent circuit changes back to the initial one.

Indeed, such periodic changes in ΔIm were observed experimentally. The increase was seen as a gradual growth in ΔIm from its initial level (*init* and *fin* in Figure 24A) followed by sharp a decrease in ΔIm, likely corresponding to completion of the bud formation and detachment of the newly formed vesicle. In the presence of a lipid reservoir, multiple changes were seen: buds formed one by one (as in Figure 24A) or the simultaneous growth of several buds was seen (as in Figure 24B). While one large buds (corresponding to level 1 in ΔIm tracing, Figure 24B) developed slowly, smaller bud can form and pinch off (e.g. note the changes of ΔIm around level 2, Figure 24B).
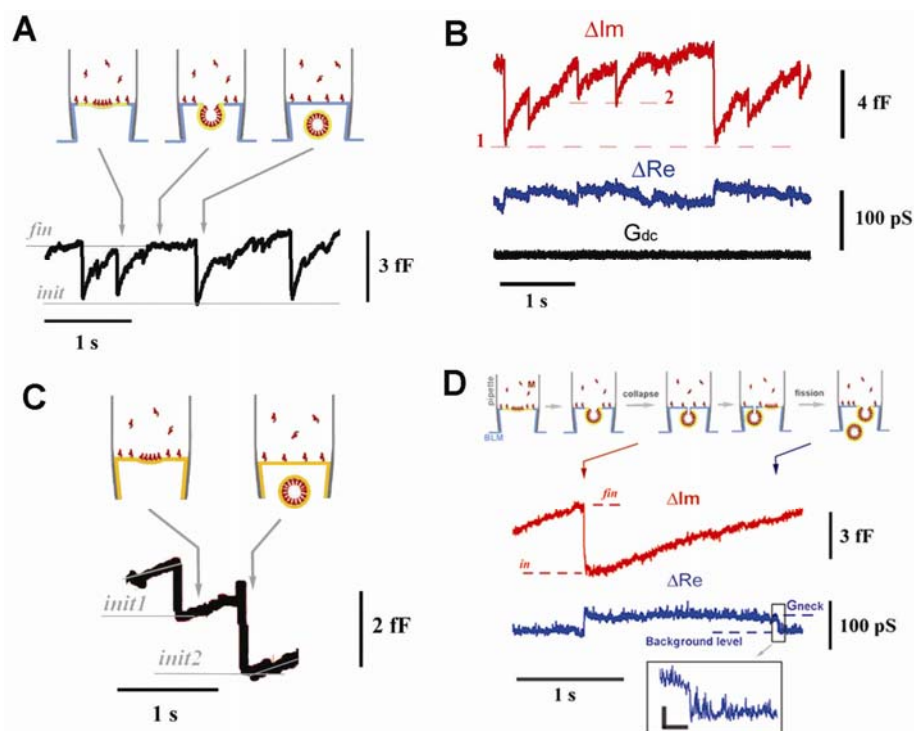

Figure 24. *Electrical admittance measurements reveal individual budding events.* **A.** Changes in the imaginary part of the admittance (ΔIm) during consecutive formation of several buds: ΔIm increases from the initial levels (*init*) until reach the final one (*fin*) during formation of a single budding vesicle; after the vesicle pinches off ΔIm returns to its initial level (see also panel D). **B.** Changes of the imaginary and real (ΔRe) parts of the admittance and ionic permeability (G_{dc}) of the membrane patch upon application of M protein (2 μM); level 1 shows the background level of ΔIm, which corresponds to the initial area of the patch; ΔIm deviations from level 1 indicate reversible changes in the patch area, when each single alteration (e.g. around level 2) indicates a budding event. **C.** Similar measurements for the patch disconnected from the membrane reservoir; note the drift of the *init* level indicating the constant decrease of the patch area. **D.** The scheme outlines changes in membrane admittance during a budding event in which a metastable membrane neck forms; levels *in* and *fin* show the ΔIm increase due to formation of a bud; in ΔRe channel the red arrow indicates bud closure, while the blue arrow indicates fission of the neck; the blow-up shows the neck fission in details.

64

The connection of the membrane patch to the external lipid reservoir was critical to see consecutive budding. Figure 24C outlines changes of the admittance in experiments with no lipid reservoir. The budding still proceeded owing to the excess lipids left on the pipette or stored in undulations of the membrane patch, but formation of buds quickly depleted these reservoirs resulting in an irreversible alteration of the patch membrane seen as a continuous decrease in the level to which ΔIm returned (Figure 24C, *init* and *init'*).

Fast drops in ΔIm did not always indicate the complete detachment of a vesicle. Rarely, after bud closure, the conductance of a thin neck connecting the bud and the membrane patch was resolved, analogous to the pinching-off of an endosome in a cellular system (Rosenboom and Lindau, 1994). When a bud starts forming, the neck conductance is very large. From equation (6) (Materials and Methods) it is seen that ΔRe is greater than zero only when the neck conductance G_n becomes comparable with the admittance of the bud membrane ($G_n/\omega C_{bud} \sim 1$), which for a typical bud size of ~100 nm corresponds to ~100 pS. Such narrow necks (few nanometers in diameter) form only at the latest stages of budding, thus for most of the process ΔRe is close to zero and only changes in ΔIm proportional to the bud capacitance (or bud area) are seen. However, Figure 24D shows a transient increase in ΔRe after the ΔIm drop, which corresponds to the formation of the neck (see equation (9) in Material and Methods). The neck conductance was detected for some time after the ΔIm drop. While ΔIm grew again due to formation of the next bud, the neck conductance dropped below the level of resolution (Figure24D, arrows). Thus, the membrane bud first closed abruptly (ΔIm drops), which was likely due to instability of the membrane connection between the forming bud and the membrane patch under tension (Frolov *et al.*, 2003). Then, the thin neck fissions or elongates so that its conductance is not resolved anymore. Usually the neck conductance drops soon after bud closure and much faster than the characteristic time of bud growth, as shown in Figure 24D. In such cases the amplitude of the ΔRe increase was much smaller than one of the preceding ΔIm drops, indicating that the neck quickly became narrow (see equivalent circuit in Figure 23 and equation (7) in Material and Methods). In such budding events the value of the ΔIm jump approached C_{bud}, proportional to the total bud area (equation (5), Material and Methods). The values of such jumps are presented in the

histogram in Figure 25A. Occasionally, fission pores were more conductive and stayed open longer, as in Figure 24B. No correlation between the value of the ΔIm jump and the fission pore behavior was obtained, indicating that the creation of membrane curvature by M protein is decoupled from membrane fission.
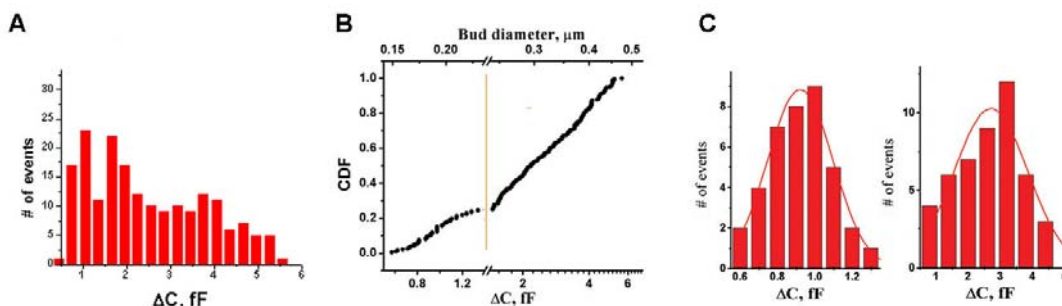

Figure 25. *Statistical analysis of the admittance measurements.* **A.** A histogram showing the amplitude distribution for ΔIm jumps detected in experiments. **B.** Cumulative distribution of the amplitude of ΔIm jumps and corresponding diameter of spherical membrane particles; initial part of the distribution (up to ~1.3 fF) is expanded to show its Gaussian-like profile. **C.** Left histogram shows the distribution of small ΔIm jumps from C; right histogram shows distribution of ΔIm jumps obtained at elevated (5 μM) concentration of M protein.

Importantly, detected admittance changes were not accompanied by any significant changes in the permeability of any membrane part within the patch pipette, as seen by the measurements of the direct current conductance (G_{dc}) of the membrane patch (Figure 24B). This finding is in agreement with the data on the hydrophobic profile of the M protein with no parts supporting extensive membrane insertion (Chambers *et al.*, 1986). The lack of leakage also supports the notion that the release of the LUV contents was not due to formation of a protein or proteolipid pores (Basanez *et al.*, 2001).

The shape of the formed bud is closer to spherical rather than to cylindrical as the access resistance (R_{pore}) remained small until the buds close up. This is further confirmed by the budding observed on GUV system. Thus, the capacitance changes measured may be transformed into final bud diameters values by following equation (5) (Materials and Methods).

If the bud is assumed spherical, then:

$$A_{bud} = \pi D_{bud}^{\;2} = \frac{C_{bud}}{C_0}, \qquad (11)$$

where D_{bud} is the diameter of the spherical bud. Then,

$$D_{bud} = \sqrt{\frac{C_{bud}}{\pi C_0}} \qquad (12)$$

Figure 25A shows capacitance values obtained, from which the bud diameters in this spherical approximation can be estimated. The values are comparable with the size of NDV particles (ranging from ~0.1 to 0.5 μm), though the distribution is broad.

The cumulative distribution function (CDF) of the values of ΔIm jumps is rather broad and skewed, with a pronounced singularity at ~1.3 fF (Figure 25B, 188 jumps in total). This singularity breaks the distribution into two parts. Smaller jumps (on the left form the break in Figure 25B) have normal size distribution, with mean value of 0.92+/-0.17 fF (SD, n=40, Figure 25C, left histogram), corresponding to a spherical bud with a diameter of ~180 nm, close to the typical sizes of NDV particle (150- 300 nm) (Takimoto and Portner, 2004). Distribution of the larger jumps is close to log-normal, ranging from 200 to 500 nm, consistent with the size heterogeneity of virus-like particles produced by M protein in cells (Pantua *et al.*, 2006) and the vesicles observed in experiments with GUVs. Increasing the M protein concentration in the pipette to 5 μM led to an overall increase in the values of ΔIm jumps (2.7+/-1.1 fF SD, n=47; Figure25C, right histogram).

Formation of vesicles from a planar bilayer with high lateral tension, σ (typically σ~10^{-3} N/m²) (Frolov *et al.*, 2003), requires substantial energy to pull lipid material from the reservoir and bend it into a sphere. For a 100 nm vesicle, such energy would reach several thousand k_BT, as:

$$\Delta E \sim 8\pi k + \sigma A_{bud}, \qquad (13)$$

where A_{bud} is the vesicle area and k is the bending modulus (as pointed in the introduction section, $k \approx 20$ k_BT for a typical phospholipid bilayer). However, if M proteins are as tightly packed on the vesicle membrane as inside the virus, the number of proteins per 100 nm vesicle is over a thousand (e.g. at 0.05 protein/lipid ratio on the membrane surface, see Figure 16B and C). At such densities the energy cost to pull material and bend it into a sphere *per protein* is low (approaching several k_BT). Thus, weak interactions between proteins and lipids in a membrane domain can sum up to provide enough energy for curvature creation. This estimation corroborates the notion that weak association of M proteins on the membrane can energetically support membrane deformations.

Besides providing required energy, the same association of M proteins controls membrane geometry producing membrane vesicles of the desired shape. Long-range coordination of membrane deformations required for vesicle formation by M protein cannot be based on the intrinsic topology of a protein lattice, as in the case of a clathrin cage, but the proteolipid interactions, possible within a budding proteo-lipid domain, may contribute to particle formation, as discussed in the introduction of this manuscript. Thus, despite its intrinsic simplicity, weak protein condensation on a membrane surface provides a powerful tool to regulate membrane shape and topology. To further investigate the nature of such budding domains, a different experimental approach was used, where the behavior of the protein on a lipid monolayer was studied.

3.5. Fluid-like behavior of domains assembled by matrix protein on lipid monolayers

As discussed in the previous section, M protein driven budding relies on the formation of proteo-lipid domains. In the introductory part of this manuscript two types of membrane domains were described: the gel-liquid phase domains (or crystalline domains) and the liquid-ordered:liquid-disordered domains (or fluid-like domains). As summarized in Table 3, the fluidity of flat membrane domains is expressed in their quasi-circular form and tendency to merge minimizing the boundary energy. Further minimization of the boundary energy is possible when domains take advantage of the third dimension and bud away. In contrast, crystalline domains have irregular shape and generally grow along certain polymerization patterns, rather than by domain merger. The data described previously provides arguments in favor of the fluidity of the M protein induced membrane domains. The bright round spots that have been identified as protein containing domains grew by merger, as can be seen from Figure 20. Admittance measurements revealed a broad distribution in the sizes of the budding vesicles. A described earlier, the merger of budding domains is likely to account for the broadness of the size distribution. However, neither the microscopic observation nor the admittance measurements directly demonstrates the microstructure of the domains. To assay finite details of the M protein membrane assemblies, electron microscopy imaging of the protein segregation on a monolayer was used. Contrary to the bilayer systems described

in detail previously, the monolayer system has intrinsic constrains to the budding activity of the protein due to the extremely high surface tension of the air-water interface. This way, the protein added to the lipid monolayer from the side of the lipid head-group will be trapped flat in two-dimensions. The results of such experiments are shown on Figure 26, where tight assembly of M proteins into circular domains on the lipid surface was confirmed on a nanometer scale by transmission electron microscopy observations. Circular patterns corresponding to aggregating proteins were detected after M protein adsorption on the lipid monolayer and no such objects were detected in control experiments when only M protein or only lipid monolayers were applied.
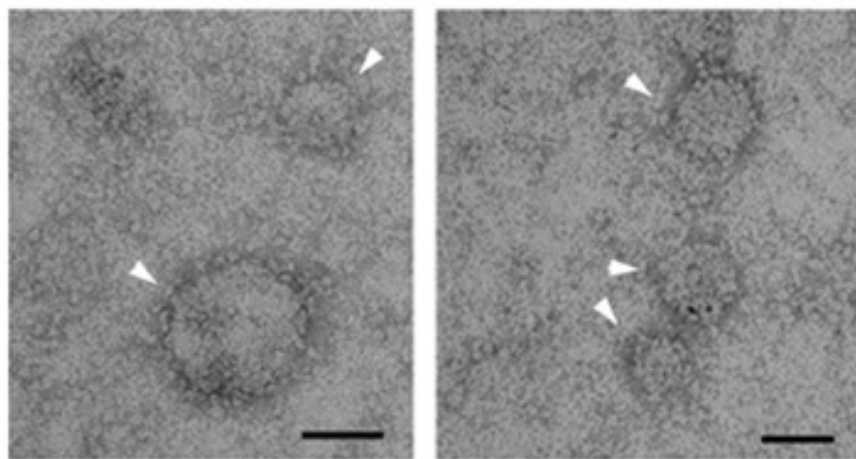
Figure 26. *Electron microscopy study of M protein condensation on a lipid monolayer.* White arrows show the round proteo-lipid domains. Bars 50 nm.

Another way to explore the fluidity of proteo-lipid domains is to measure changes in the lipid monolayer surface pressure induced by the protein. This was done using the Wilhelmy balance as described in materials and methods. The typical plot of surface pressure versus area per molecule of a DOPC monolayer containing 10% of cholesterol is seen as a solid line in Figure 27A. Here the transition from the gas phase into a liquid phase is indicated by the change in the slope of the curve before the monolayer collapse. When M protein was added into the subphase in the presence of such monolayer, the slope of the plot developed a new kink around 12 mN/m (dashed line in Figure 27A).

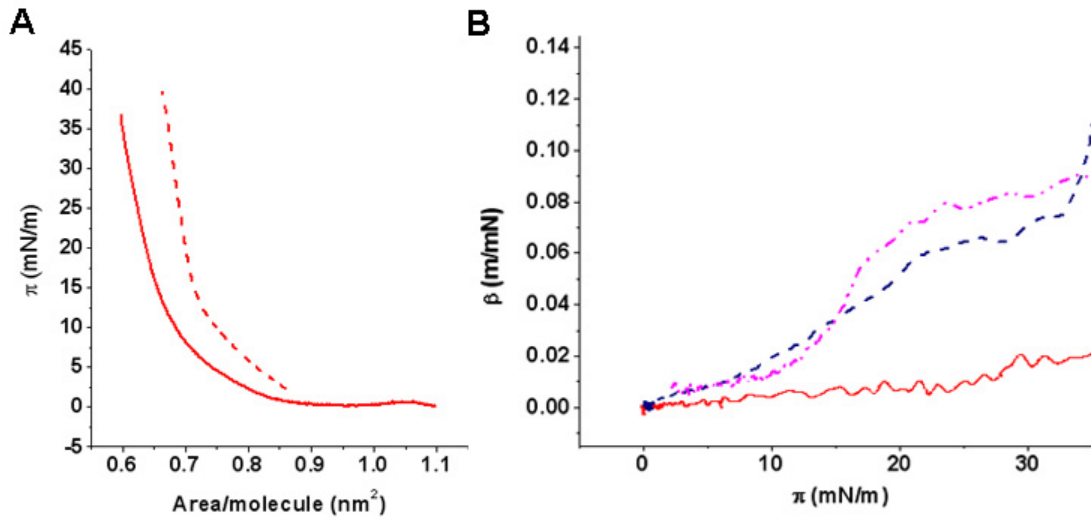**Figure 27.** *Interaction of M protein with lipid monolayer on air-water interface.* **A.** Surface pressure-area isotherms (at room temperature) of pure DOPC:Cholesterol (9:1, 0.27 mM) monolayer (solid line) and of DOPC:Cholesterol (9:1, 0.27 mM) monolayer compressed in the presence of 0.54 nM of M protein (dashed line); in the latter experiments the lipid monolayer was pre-formed in the absence of the protein and then compressed after addition of the protein. **B.** β-π plot for pure M protein (0.54 nM; red solid line), DOPC:Cholesterol monolayer (0.27 mM; blue dash line) and M protein (0.54 nM) applied to a pre-formed DOPC:Cholesterol monolayer (0.27 mM; magenta, dash-doted line).

These data can be re-plotted as the compressibility coefficient versus surface pressure (Kamilya *et al.*, 2007) (Figure 27B), where the compressibility coefficient is defined as:

$$\beta = -\left(\frac{1}{A}\right) \times \left(\frac{\delta A}{\delta \pi}\right)_T, \qquad (14)$$

where A is the area per molecule and π is the surface pressure. It is interesting to note that M protein adsorbed only weakly onto the air-water interface in the absence of the lipid monolayer (Figure 27B, solid line). For the pure lipid monolayer, the compressibility coefficient grew slightly until reach a maximum around 26 mN/m before the collapse of the film (Figure 27B, dash line). Addition of the protein to a pre-compressed lipid monolayer (Material and Methods) changed the behavior of the β (Figure 27B, dash-dot line). First, a plateau was seen until the surface pressure reached ~12 mN/m. At this point, which corresponds to the kink in Figure 27A, a very pronounced growth in the curve slope occurred until reaching a maximum at 26 mN/m. The asymmetry of the curve indicates that phase transitions could proceed in several steps.

These data strongly indicate that the lipid monolayers with bound M proteins have an additional phase transition point in comparison with the pure lipid film. If a

solidification of the monolayer happened (e.g. formation of a crystalline or gel phase induced by the protein adsorption), the surface pressure values near the new kink should be much higher (usually at 30-40 mN/m) (Cruz and Perez-Gil, 2007). Rather, low surface pressure value at the new kink (~12 mN/m) indicates ordering of the liquid phase (consistently with formation of fluid-like proteo-lipid domains). The maximum value of the compressibility coefficient is larger in the presence of the protein, which indicates higher intermolecular cooperativity in the proteo-lipid film (Kamilya *et al.*, 2007). Altogether, the experiments on M protein interaction with lipid monolayers provide additional arguments toward the fluidity of the M protein-lipid domains observed by other techniques.

3.6. Modeling a proteo-lipid fluid domain budding: simple energy considerations

The experimental data presented above were further analyzed theoretically in the framework of Lipowsky's model for the budding of a membrane fluid domain (Lipowsky, 1992) (see Introduction section). In this model, the energy of a fluid domain budding from a lipid membrane is equal to the sum of the bending energy of the bilayer plus the edge energy of the domain (originating from the line tension on the domain periphery).

$$E_{Lip} = (E_{bend} + E_{edge}) \qquad (15)$$

If the domain forms a spherical cap with curvature C (radius of curvature R=1/C) and opening radius N (*Figure 28*), then the *bending energy* of the domain is given by:

$$E_{bend} = \frac{Ak}{2}(2C - 2C_{sp})^2 = 2\pi k(LC - LC_{sp})^2 \qquad (16)$$

where A is the surface area (A=πL^2, see Figure 14) and *k* is the bending rigidity of the membrane, that for typical phospholipids bilayers has a value of ~ 10^{-19} J $\approx$ 24 $k_B T$ (Lipowsky, 1992).
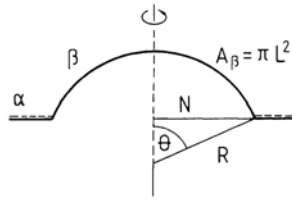
Figure 28. *Geometrical parameters of a membrane domain (b) forming a spherical bud.* The area of the bud is defined as $A_\beta = \pi L^2$, the bud curvature as $C=1/R$ and the neck radius is N. Adapted from Lipowsky, 1992.

The *edge energy* of the domain is given by:

$$E_{edge} = \sigma 2\pi N = \sigma 2\pi L\sqrt{1-(LC/2)^2} \qquad (17)$$

where σ denotes line tension of the domain boundary. For lipid domains the value of the line tension can be estimated as 10^{-11}N (Lipowsky, 1992). However, the line tension can be different for domains assembled with the help of proteins (such as M protein molecules). The edge length is defined as 2πN, where N = $L\sqrt{1-(LC/2)^2}$ (Lipowsky, 1992).

As postulated by Lipowsky: "a flat domain with surface area A embedded in a flat membrane matrix will form a circular disk of radius L = $(A/\pi)^2$ in order to attain a state with a minimal value, 2πL, for the length of its edge. The edge can be further reduced if the domain deforms into the "third dimension" and form a bud". However, as noted by Lipowsky, to perform budding the domain should reach a certain size (L_c), so that the edge energy exceeded the curvature energy of the bud. Figure 29A illustrates the dependence of this energy defined by Lipowsky (E_{Lip}) on the domain curvature (LC) for domains of different size. All curves have two similar minima (at ±2 LC) which correspond to closed vesicles budded in opposite directions from the membrane plane. The minimum at LC=0, indicating a stable flat (C=0) domain, is seen for small domains (Figure 29A, red curve), but absent from larger domains (Figure 29A, blue curve). The black curve (Figure 29A) corresponds to the critical size of the domain (L_c) at which the minimum at LC=0 disappears.
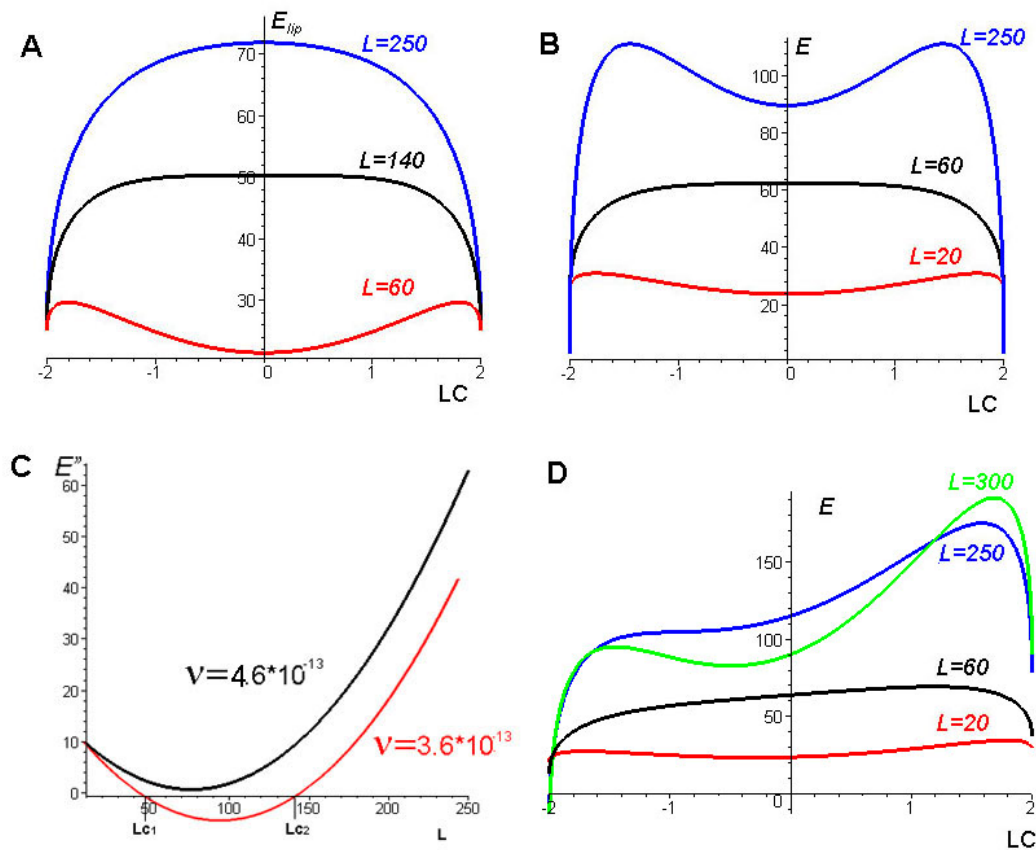
Figure 29. *Fluid domain budding: energy components consideration.* **A.** Dependence of the domain energy defined by Lipowsky in absence of line tension (E_{Lip}) on curvature (LC) for domains of different sizes. Budding occurs in the extreme minima. The minimum at LC=0, that appear for smaller domain (red curve) indicates stable flat domains. This minimum does not exist in larger domains (blue curve). The black curve corresponds to the critical size of the domain, at which the minimum at LC=0 disappears. Domain spontaneous curvature is considered zero. **B.** Behavior of the energy that includes the line tension term as a function of LC for different L. The minimum at LC=0 appears at higher L values, indicating that large flat domains are as stable as the small ones. Domain spontaneous curvature is considered zero. **C.** Second derivation of the energy from B over L (E"(L)) at LC=0. The E"(L) dependence is showed for two values of the lateral tension. For large tension E"(L) is always positive, so that flat domains are stable. For small tension, a region of instability appears (from L_{c1} to L_{c2}) where growing domains bud spontaneously, as the energy had a maximum for that L values. **D.** Behavior of the energy as a function of LC when a non-zero spontaneous curvature of the growing domain is considered. The inclusion of a small negative spontaneous curvature into the energy equation (2% difference in cholesterol concentration between the membrane monolayers is considered for the plot represented) produces a broadening of the size distribution of the resulting buds toward. The energy curvature presents pronounced asymmetry, thus securing the unidirectional budding toward the negative curvature.

Though this theory was created for purely lipidic fluid domains, the same principles can be applied to describe budding of fluid domains formed by M protein. In this case the line tension occurs on the boundary of the proteolipid domains (seen in Figure 20 or 26) created by M proteins. For simplification, it is further assumed that M proteins influence the bending energy of the proteolipid domain via modification of its spontaneous

curvature C_{sp}, However, two more energy terms should be taken into account. First, when a vesicle is formed from a lipid bilayer connected to a reservoir (e.g. BLM, Figure 24), the surface tension (σ) of the membrane has to be included. Second, the energy of M protein association into a domain should be taken into account. If the difference in chemical potentials for a protein inside and outside of the domain ($\mu-\mu_0$) is assumed fixed, the association energy will be simply proportional to the domain area. These two terms constitute the *surface energy* of the domain:

$$E_{surf} = \gamma\left(\pi L^2 - \pi N^2\right) + \frac{\pi L^2}{a}(\mu-\mu_0) = \pi L^2\gamma(LC/2)^2 + \frac{\pi L^2}{a}(\mu-\mu_0),\qquad (18)$$

where γ is the surface tension of the membrane and a is the area occupied by M protein on the membrane. The measured value of γ for membranes used in this work varies between $\sim 10^{-13}$ N/nm (BLM) and $0.1*10^{-13}$ N/nm (GUV). In the framework of this simple analysis, a value of $4*10^{-13}$ N/nm is used. The total energy of the domain can be rewritten as:

$$E = (E_{bend} + E_{edge} + E_{surf})\qquad (19)$$

Combining formulae 16-19, the total energy of the domain, normalized for k, is:

$$E = 2\pi((LC-LC_{sp})^2 + (L/\xi)\sqrt{1-(LC/2)^2} + (L/\xi')^2(L/C)^2 - L^2\xi''),\qquad (20)$$

where $\xi=k/\sigma$, $\xi'=\sqrt{8k/\gamma}$ and $\xi''=(\mu-\mu_0)/2a\sigma$. For convenience, this energy will be presented in k_BT units where T is the temperature in Kelvins and k_B is the Boltzmann constant.

In Figure 29B the behavior of *E* as a function of *LC* is presented for different *L*. As in the case of lipid domains presented above (Figure 29A), the spontaneous curvature of the domain is neglected. Figure 29B shows that budding is possible only for certain range of *L* values: the minimum at LC=0, seen for small domains in Lipowsky model, appears at large L values, indicating that large flat domains become stabilized by lateral tension of the membrane. This range of *L* is determined by the ratio between line and lateral tensions and bending rigidity of the domain. If the minimum at LC=0 exists, then the second derivation of *E"* over *L* at LC=0 ($E_{LL}^{ll}(LC=0)$) should be negative. The dependence of $E_{LL}^{ll}(LC=0)$ on *L* is showed on Figure 29C for different values of the lateral tension. For large tensions *E"* is always positive so that flat domains are stable. For smaller tensions a region of instability appears (Figure 29C, from L_{c1} to L_{c2}) where

growing domains bud spontaneously. This region is centered at ~150 nm (comparable with experimentally observed values for M protein domains), for an intermediate tension (0.3-0.5 dyn/cm), bending rigidity of 50-70kT and a line tension of 70 pN.

In the experiments with M protein, the vesicles formed in a unidirectional way toward the negative curvature of the bud (Figures 19, 20 and 22). M proteins interact directly only with one monolayer of the membrane, thus the budding proceeds asymmetrically and the spontaneous curvature of the growing domain should be also taken into account. Introducing the non-zero spontaneous curvature changed slightly the effect of the lateral tension described above. As can be observed in Figure 29D, the region of spontaneous budding of the growing domain is now slightly expanded toward larger domain sizes (e.g. the intermediate minimum does not appear until bigger L value, Figure 29D, green line), thus making the size distribution of the resulting buds broader. Importantly, the energy curve is now skewed to one side so that creation of buds with negative curvature is promoted (Figure 29D). Notably, only minor changes in spontaneous curvature induce pronounced asymmetry in the energy curve, thus securing the unidirectional budding. Such changes can be due, for example, to small asymmetry in cholesterol distribution introduced by M proteins.

Finally, to illustrate the whole budding process the energy dependence on *L* and *LC* is presented in Figure 30. Domains grow to cross the energy barrier and then either bud (Figure 30, red arrow to the left) or continue growing flat (Figure 30, white arrow). This implies other mechanisms for the formation of bigger vesicles. As the budding domains are considered fluid, these bigger vesicles may form by merging of smaller domains in order to avoid the high energy cost of direct domain budding. But this mechanism is outside of the framework of the present model.

In conclusion, the model presented here supports the idea of membrane budding by fluid proteolipid domains. The size of the budding vesicles is controlled not via a scaffold of predetermined geometry, but via a careful balance between different forces defining the energetics of the budding process. The energy per protein needed for a proteolipid domain to undergo budding is of the order of a few k_BT, in accordance with the result obtained by the theoretical work on fluid domain budding (Lipowsky, 1992). The intrinsic curvature of the proteolipid fluid domain provides unidirectionality to the process and also results in lowering of the energy per protein required for budding of the
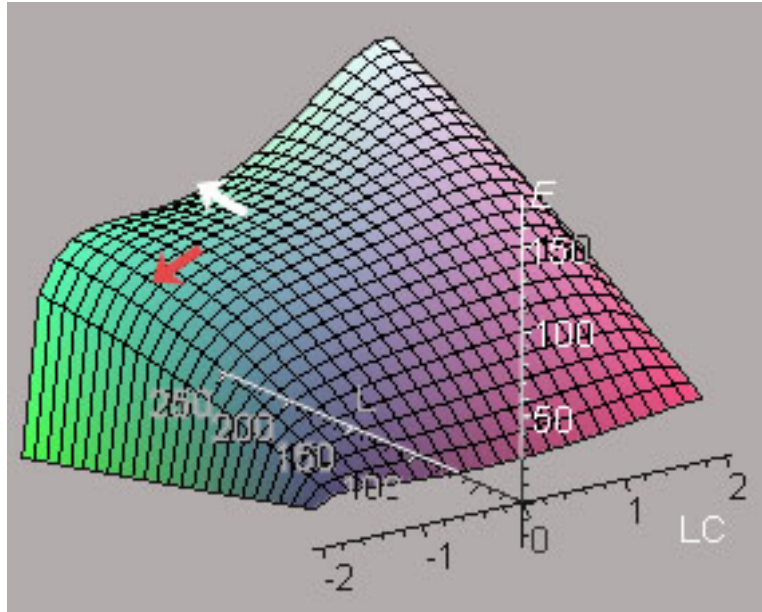
Figure 30. *Three dimentional representation of the energy dependence of the budding process on the size and curvature of the growing domain.* Domains should grow to reach certain size and cross the energy barrier. After that point, the domain may choose between budding (indicated as red arrow to the left) or continue growing flat (white arrow).

smallest proteolipid vesicles. The spontaneous curvature may come from cholesterol segregation with the M protein. Also, experimental data suggest that in the absence of cholesterol, M protein may induce budding if DOPE is present in the system (Figure 22). DOPE has larger negative spontaneous curvature than cholesterol, so smaller redistributions of this lipid will lead to the same result of unidirectionality of budding. However, the ability of M protein to induce unidirectional budding of charged membranes without the presence of any lipid with negative curvature, suggest that membrane assembly of M proteins imposes negative curvature independently on the lipids. This ability is to be explored more deeply in future studies.

In order to shake a hypothesis, it is sometimes not necessary to do anything more than push it as far as it will go.

Denis Diderot

IV. CONCLUSIONS

1. Matrix protein of Newcastle Disease Virus is sufficient to produce membrane budding upon its adsorption on a lipid membrane. The size distribution of the vesicles budded from the lipid membrane is in good agreement with the size distribution of viral particles produced *in vivo*. Thus, M protein possesses the energy and the intrinsic geometrical information to induce budding in cells without the help of other cellular machineries.

2. M protein of NDV organizes domains on the lipid membrane. Lipids in such domains have limited mobility and the components of the system organize into a new fluid-like phase, as evidenced by their rounded shape and ability to fuse together.

3. Fluid-like domains originated by NDV matrix protein interaction with the membrane evolve by budding, confirming that the mechanism of domain driven budding is applicable for budding of enveloped viruses.

4. NDV matrix protein binding and budding are dependent on the membrane lipid composition. While binding is enhanced by the presence of lipids with negative curvature, such as cholesterol or DOPE, it is not affected by the presence of charge in the membrane; the budding activity is enhanced in both cases.

5. Budding of lipid membrane induced by its interaction with NDV matrix protein is unidirectional. Thus, matrix protein induces negative curvature upon its self-assembly on the membrane template. A model of unidirectional budding induced by NDV matrix protein indicates lipid distribution asymmetry, such as cholesterol concentration in one of the lipid leaflets, as an additional factor that contributes to the effectiveness of budding.

V. BIBLIOGRAPHY

Adams, W.R. and A.M. Prince (1957).
"An electron microscopic study of incomplete virus formation; infection of Ehrlich ascites tumor cells with chick embryo-adapted Newcastle disease virus (NDV)."
J Exp Med **106**(5):617-26

Alexander, D.J. (2000).
"Newcastle disease and other avian paramyxoviruses."
Rev Sci Tech **19**(2):443-62

Alexander, D.J., R.J. Manvell, K.M. Frost, W.J. Pollitt, D. Welchman and K. Perry (1997).
"Newcastle disease outbreak in pheasants in Great Britain in May 1996."
Vet Rec **140**(1):20-2

Angelova, M.I. and D.S. Dimitrov (1988).
"A mechanism of liposome electroformation."
Prog. Colloid. Polym. Sci. **76**:59-67

Antonny, B., P. Gounon, R. Schekman and L. Orci (2003).
"Self-assembly of minimal COPII cages."
EMBO Rep **4**(4):419-24

Baba, T., C. Rauch, M. Xue, N. Terada, Y. Fujii, H. Ueda, I. Takayama, S. Ohno, E. Farge and S.B. Sato (2001).
"Clathrin-dependent and clathrin-independent endocytosis are differentially sensitive to insertion of poly (ethylene glycol)-derivatized cholesterol in the plasma membrane."
Traffic **2**(7):501-12

Babst, M. (2005).
"A protein's final ESCRT."
Traffic **6**(1):2-9

Basanez, G., J. Zhang, B.N. Chau, G.I. Maksaev, V.A. Frolov, T.A. Brandt, J. Burch, J.M. Hardwick and J. Zimmerberg (2001).
"Pro-apoptotic cleavage products of Bcl-xL form cytochrome c-conducting pores in pure lipid membranes."
J Biol Chem **276**(33):31083-91

Bauer, M. and L. Pelkmans (2006).
"A new paradigm for membrane-organizing and -shaping scaffolds."
FEBS Lett **580**(23):5559-64

Baumgart, T., S.T. Hess and W.W. Webb (2003).
"Imaging coexisting fluid domains in biomembrane models coupling curvature and line tension."
Nature **425**(6960):821-4

Bonifacino, J.S. and B.S. Glick (2004).
"The mechanisms of vesicle budding and fusion."
Cell **116**(2):153-66

Boucher, J., E. Trudel, M. Methot, P. Desmeules and C. Salesse (2007).
"Organization, structure and activity of proteins in monolayers."
Colloids Surf B Biointerfaces **58**(2):73-90

Briggs, J.A., T. Wilk and S.D. Fuller (2003).
"Do lipid rafts mediate virus assembly and pseudotyping?"
J Gen Virol **84**:757-68

Brugger, B., B. Glass, P. Haberkant, I. Leibrecht, F.T. Wieland and H.G. Krausslich (2006).
"The HIV lipidome: a raft with an unusual composition."
Proc Natl Acad Sci U S A **103**(8):2641-6

Chambers, P., N.S. Millar, S.G. Platt and P.T. Emmerson (1986).
"Nucleotide sequence of the gene encoding the matrix protein of Newcastle disease virus."
Nucleic Acids Res **14**(22):9051-61

Chen, B.J. and R.A. Lamb (2008).
"Mechanisms for enveloped virus budding: Can some viruses do without an ESCRT?"
Virology **372**(2):221-32

Chen, C., J. Jin, M. Rubin, L. Huang, T. Sturgeon, K.M. Weixel, D.B. Stolz, S.C. Watkins, J.R. Bamburg, O.A. Weisz and R.C. Montelaro (2007).
"Association of Gag Multimers with Filamentous Actin During Equine Infectious Anemia Virus Assembly."
Current HIV Research **5**:315-323

Coorssen, J.R., P.S. Blank, F. Albertorio, L. Bezrukov, I. Kolosova, P.S. Backlund, Jr. and J. Zimmerberg (2002).
"Quantitative femto- to attomole immunodetection of regulated secretory vesicle proteins critical to exocytosis."
Anal Biochem **307**(1):54-62

Couet, J., M.M. Belanger, E. Roussel and M.C. Drolet (2001).

"Cell biology of caveolae and caveolin."
Adv Drug Deliv Rev **49**(3):223-35

Cruz, A. and J. Perez-Gil (2007).
"Langmuir films to determine lateral surface pressure on lipid segregation."
Methods Mol Biol **400**:439-57

Curran, J. and D. Kolakofsky (1999).
"Replication of paramyxoviruses."
Adv Virus Res **54**:403-22

Danielli, J.F. and H. Davson (1935).
"A contribution to the theory of permeability of thin films."
J. Cellular Comp. Physiol. **7**:393-408

DiNapoli, J.M., L. Yang, A. Suguitan, Jr., S. Elankumaran, D.W. Dorward, B.R. Murphy, S.K. Samal, P.L. Collins and A. Bukreyev (2007).
"Immunization of primates with a Newcastle disease virus-vectored vaccine via the respiratory tract induces a high titer of serum neutralizing antibodies against highly pathogenic avian influenza virus."
J Virol **81**(21):11560-8

Engelman, D.M. (2005).
"Membranes are more mosaic than fluid."
Nature **438**(7068):578-80

Epand, R.M. (2007).
"Membrane lipid polymorphism: relationship to bilayer properties and protein function."
Methods Mol Biol **400**:15-26

Faaberg, K.S. and M.E. Peeples (1988).
"Association of soluble matrix protein of Newcastle disease virus with liposomes is independent of ionic conditions."
Virology **166**(1):123-32

Ford, M.G., I.G. Mills, B.J. Peter, Y. Vallis, G.J. Praefcke, P.R. Evans and H.T. McMahon (2002).
"Curvature of clathrin-coated pits driven by epsin."
Nature **419**(6905):361-6

Ford, M.G., B.M. Pearse, M.K. Higgins, Y. Vallis, D.J. Owen, A. Gibson, C.R. Hopkins, P.R. Evans and H.T. McMahon (2001).
"Simultaneous binding of PtdIns(4,5)P2 and clathrin by AP180 in the nucleation of clathrin lattices on membranes."

Science **291**(5506):1051-5

Fraley, R., S. Subramani, P. Berg and D. Papahadjopoulos (1980).
"Introduction of liposome-encapsulated SV40 DNA into cells."
J Biol Chem **255**(21):10431-5

Frick, M., N.A. Bright, K. Riento, A. Bray, C. Merrified and B.J.
Nichols (2007).
"Coassembly of flotillins induces formation of membrane
microdomains, membrane curvature, and vesicle budding."
Curr Biol **17**(13):1151-6

Frolov, V.A., V.A. Lizunov, A.Y. Dunina-Barkovskaya, A.V.
Samsonov and J. Zimmerberg (2003).
"Shape bistability of a membrane neck: a toggle switch to control
vesicle content release."
Proc Natl Acad Sci U S A **100**(15):8698-703

Garcia-Sastre, A., J.A. Cabezas and E. Villar (1989).
"Proteins of Newcastle disease virus envelope: interaction between
the outer hemagglutinin-neuraminidase glycoprotein and the inner
non-glycosylated matrix protein."
Biochim Biophys Acta **999**(2):171-5

Garoff, H., R. Hewson and D.J. Opstelten (1998).
"Virus maturation by budding."
Microbiol Mol Biol Rev **62**(4):1171-90

Giuffre, R.M., D.R. Tovell, C.M. Kay and D.L. Tyrrell (1982).
"Evidence for an interaction between the membrane protein of a
paramyxovirus and actin."
J Virol **42**(3):963-8

Gortel, E. and F. Grendel (1935).
"On biomolecular layers of lipoids on chromatocytes of blood."
J. Exp. Medicine **41**:439-443

Gruner, S.M., P.R. Cullis, M.J. Hope and C.P. Tilcock (1985).
"Lipid polymorphism: the molecular basis of nonbilayer phases."
Annu Rev Biophys Biophys Chem **14**:211-38

Han, G.Z., C.Q. He, N.Z. Ding and L.Y. Ma (2008).
"Identification of a natural multi-recombinant of Newcastle disease
virus."
Virology **371**(1):54-60

Han, Z. and R. Harty (2005).
"Packaging of actin into Ebola virus VLPs."

Virology Journal **2**(1):92

Hanson, P.I., R. Roth, Y. Lin and J.E. Heuser (2008).
"Plasma membrane deformation by circular arrays of ESCRT-III protein filaments."
J Cell Biol **180**(2):389-402

Harden, J.L., F.C. Mackintosh and P.D. Olmsted (2005).
"Budding and domain shape transformations in mixed lipid films and bilayer membranes."
Phys Rev E Stat Nonlin Soft Matter Phys **72**(1):011903

Helfrich, W. (1973).
"Elastic properties of lipid bilayers: theory and possible experiments."
Z Naturforsch [C] **28**(11):693-703

Henriksen, J., A.C. Rowat and J.H. Ipsen (2004).
"Vesicle fluctuation analysis of the effects of sterols on membrane bending rigidity."
Eur Biophys J **33**(8):732-41

Higgins, M.K. and H.T. McMahon (2005).
"In vitro reconstitution of discrete stages of dynamin-dependent endocytosis."
Methods Enzymol **404**:597-611

Horvath, J.C., A. Horak, J.G. Sinkovics, M. Pritchard, S. Pendleton and E. Horvath (1999).
"Cancer vaccines with emphasis on a viral oncolysate melanoma vaccine."
Acta Microbiol Immunol Hung **46**(1):1-20

Hurley, J.H. (2008).
"ESCRT complexes and the biogenesis of multivesicular bodies."
Current Opinion in Cell Biology
Cell structure and dynamics **20**(1):4-11

Hurley, J.H. and S.D. Emr (2006).
"The ESCRT complexes: structure and mechanism of a membrane-trafficking network."
Annu Rev Biophys Biomol Struct **35**:277-98

Israelachvili, J.N. (1977).
"Refinement of the fluid-mosaic model of membrane structure."
Biochim Biophys Acta **469**(2):221-5

Jamieson, J.D. and G.E. Palade (1967a).

"Intracellular transport of secretory proteins in the pancreatic exocrine cell. I. Role of the peripheral elements of the Golgi complex."
J Cell Biol **34**(2):577-96

Jamieson, J.D. and G.E. Palade (1967b).
"Intracellular transport of secretory proteins in the pancreatic exocrine cell. II. Transport to condensing vacuoles and zymogen granules."
J Cell Biol **34**(2):597-615

Janke, M., B. Peeters, O. de Leeuw, R. Moorman, A. Arnold, P. Fournier and V. Schirrmacher (2007).
"Recombinant Newcastle disease virus (NDV) with inserted gene coding for GM-CSF as a new vector for cancer immunogene therapy."
Gene Ther **14**(23):1639-49

Jayakar, H.R., E. Jeetendra and M.A. Whitt (2004).
"Rhabdovirus assembly and budding."
Virus Res **106**(2):117-32

Jin, A.J., K. Prasad, P.D. Smith, E.M. Lafer and R. Nossal (2006).
"Measuring the elasticity of clathrin-coated vesicles via atomic force microscopy."
Biophys J **90**(9):3333-44

Jouvenet, N., S.J. Neil, C. Bess, M.C. Johnson, C.A. Virgen, S.M. Simon and P.D. Bieniasz (2006).
"Plasma membrane is the site of productive HIV-1 particle assembly."
PLoS Biol **4**(12): e435

Kamilya, T., P. Pal and G.B. Talapatra (2007).
"Interaction of ovalbumin with phospholipids Langmuir-Blodgett film."
J Phys Chem B **111**(5):1199-205

Kirkham, M. and R.G. Parton (2005).
"Clathrin-independent endocytosis: new insights into caveolae and non-caveolar lipid raft carriers."
Biochim Biophys Acta **1746**(3):349-63

Laliberte, J.P., L.W. McGinnes and T.G. Morrison (2007).
"Incorporation of Functional HN-F Glycoprotein-Containing Complexes into Newcastle Disease Virus Is Dependent on Cholesterol and Membrane Lipid Raft Integrity"
J. Virol. **81**(19):10636-10648

Langhorst, M.F., A. Reuter and C.A. Stuermer (2005).
"Scaffolding microdomains and beyond: the function of reggie/flotillin proteins."
Cell Mol Life Sci **62**(19-20):2228-40

Li, J.K., T. Miyakawa and C.F. Fox (1980).
"Protein organization in Newcastle disease virus as revealed by perturbant treatment."
J Virol **34**(1):268-71

Li, L. and J.X. Cheng (2006).
"Coexisting stripe- and patch-shaped domains in giant unilamellar vesicles."
Biochemistry **45**(39):11819-26

Lipowsky, R. (1992).
"Budding of membranes induced by intramembrane domains."
J. Phys. II France **2**:1825-40

Lollike, K. and M. Lindau (1999).
"Membrane capacitance techniques to monitor granule exocytosis in neutrophils."
J Immunol Methods **232**(1-2):111-20

Lomniczi, B., E. Wehmann, J. Herczeg, A. Ballagi-Pordany, E.F. Kaleta, O. Werner, G. Meulemans, P.H. Jorgensen, A.P. Mante, A.L. Gielkens, I. Capua and J. Damoser (1998).
"Newcastle disease outbreaks in recent years in western Europe were caused by an old (VI) and a novel genotype (VII)."
Arch Virol **143**(1):49-64

Mallabiabarrena, A. and V. Malhotra (1995).
"Vesicle biogenesis: the coat connection."
Cell **83**(5):667-9

Markwell, M.A., S.M. Haas, L.L. Bieber and N.E. Tolbert (1978).
"A modification of the Lowry procedure to simplify protein determination in membrane and lipoprotein samples."
Anal Biochem **87**(1):206-10

Marsh, M. and H.T. McMahon (1999).
"The structural era of endocytosis."
Science **285**(5425):215-20

Martin, S. and R.G. Parton (2005).
"Caveolin, cholesterol, and lipid bodies."
Semin Cell Dev Biol **16**(2):163-74

Marushchak, D., S. Kalinin, I. Mikhalyov, N. Gretskaya and A.J. LB (2006).
"Pyrromethene dyes (BODIPY) can form ground state homo and hetero dimers: photophysics and spectral properties."
Spectrochim Acta A Mol Biomol Spectrosc **65**(1):113-22

Matsuo, H., J. Chevallier, N. Mayran, I. Le Blanc, C. Ferguson, J. Faure, N.S. Blanc, S. Matile, J. Dubochet, R. Sadoul, R.G. Parton, F. Vilbois and J. Gruenberg (2004).
"Role of LBPA and Alix in multivesicular liposome formation and endosome organization."
Science **303**(5657):531-4

Mayer, L.D., M.J. Hope and P.R. Cullis (1986).
"Vesicles of variable sizes produced by a rapid extrusion procedure."
Biochim Biophys Acta **858**(1):161-8

McCreedy, B.J., Jr., K.P. McKinnon and D.S. Lyles (1990).
"Solubility of vesicular stomatitis virus M protein in the cytosol of infected cells or isolated from virions."
J Virol **64**(2):902-6

McMahon, H.T. and J.L. Gallop (2005).
"Membrane curvature and mechanisms of dynamic cell membrane remodelling."
Nature **438**(7068):590-596

McMahon, H.T. and I.G. Mills (2004).
"COP and clathrin-coated vesicle budding: different pathways, common approaches."
Curr Opin Cell Biol **16**(4):379-91

Melikov, K.C., V.A. Frolov, A. Shcherbakov, A.V. Samsonov, Y.A. Chizmadzhev and L.V. Chernomordik (2001).
"Voltage-induced nonconductive pre-pores and metastable single pores in unmodified planar lipid bilayer."
Biophys J **80**(4):1829-36

Mouritsen, O.G. (2005) *Life-as a Matter of fat:The emerging science of lipidomics,* Springer-Verlag New York, LLC.

Mueller, P. and D.O. Rudin (1967).
"Action potential phenomena in experimental bimolecular lipid membranes."
Nature **213**(5076):603-4

Mui, B.L., P.R. Cullis, E.A. Evans and T.D. Madden (1993).
"Osmotic properties of large unilamellar vesicles prepared by extrusion."
Biophys J **64**(2):443-53

Mullen, J.T. and K.K. Tanabe (2002).
"Viral oncolysis."
Oncologist **7**(2):106-19

Neher, E. and B. Sakmann (1992).
"The patch clamp technique."
Sci Am **266**(3):44-51

Neitchev, V.Z. and L.P. Dumanova (1992).
"Effects of the components of Newcastle disease virus on the structural order of lipid assemblies."
Mol Biol Rep **16**(1):27-31

Palade, G. (1975).
"Intracellular Aspects of the Process of Protein Synthesis."
Science **189**(4200): 347-58

Palade, G.E. (1953).
"An electron microscope study of the mitochondrial structure."
J Histochem Cytochem **1**(4):188-211

Pantua, H.D., L.W. McGinnes, M.E. Peeples and T.G. Morrison (2006).
"Requirements for the assembly and release of Newcastle disease virus-like particles."
J Virol **80**(22):11062-73

Parton, R.G. and K. Simons (2007).
"The multiple faces of caveolae."
Nat Rev Mol Cell Biol **8**(3):185-94

Peeples, M.E. and M.A. Bratt (1984).
"Mutation in the matrix protein of Newcastle disease virus can result in decreased fusion glycoprotein incorporation into particles and decreased infectivity."
J Virol **51**(1):81-90

Polozov, I.V., L. Bezrukov, K. Gawrisch and J. Zimmerberg (2008).
"Progressive ordering with decreasing temperature of the phospholipids of influenza virus."
Nat Chem Biol **4**(4):248-55

Puhler, F., J. Willuda, J. Puhlmann, D. Mumberg, A. Romer-Oberdorfer and R. Beier (2008).
"Generation of a recombinant oncolytic Newcastle disease virus and expression of a full IgG antibody from two transgenes."
Gene Ther **15**(5): 371-83

Ratinov, V., I. Plonsky and J. Zimmerberg (1998).
"Fusion pore conductance: experimental approaches and theoretical algorithms."
Biophys J **74**(5):2374-87

Reynwar, B.J., G. Illya, V.A. Harmandaris, M.M. Muller, K. Kremer and M. Deserno (2007).
"Aggregation and vesiculation of membrane proteins by curvature-mediated interactions."
Nature **447**(7143):461-4

Robertson, J.D. (1966).
"Granulo-fibrillar and globular substructure in unit membranes."
Ann N Y Acad Sci **137**(2):421-40

Robinson, M.S. (1997).
"Coats and vesicle budding."
Trends Cell Biol **7**(3):99-102

Rosenboom, H. and M. Lindau (1994).
"Exo-endocytosis and closing of the fission pore during endocytosis in single pituitary nerve terminals internally perfused with high calcium concentrations."
Proc Natl Acad Sci U S A **91**(12):5267-71

Rothenberg, S.P., D. Kyner and G. Solomon (1992).
"Identification of a novel reductase in folate metabolism."
Mt Sinai J Med **59**(2):150-3

Russell, P.H. and J.D. Almeida (1984).
"A regular subunit pattern seen on non-infectious Newcastle disease virus particles."
J Gen Virol **65** (6):1023-31

Sackmann, E. (1994).
"The seventh Datta Lecture. Membrane bending energy concept of vesicle- and cell-shapes and shape-transitions."
FEBS Lett **346**(1):3-16

Sagrera, A., C. Cobaleda, S. Berger, M.J. Marcos, V. Shnyrov and E. Villar (1998).

"Study of the influence of salt concentration on Newcastle disease virus matrix protein aggregation."
Biochem Mol Biol Int **46**(3):429-35

Samsonov, A.V., I. Mihalyov and F.S. Cohen (2001).
"Characterization of cholesterol-sphingomyelin domains and their dynamics in bilayer membranes."
Biophys J **81**(3):1486-500

Scheid, A. and P.W. Choppin (1973).
"Isolation and purification of the envelope proteins of Newcastle disease virus."
J Virol **11**(2):263-71

Seal, B.S., D.J. King and R.J. Meinersmann (2000).
"Molecular evolution of the Newcastle disease virus matrix protein gene and phylogenetic relationships among the paramyxoviridae."
Virus Research **66**(1):1-11

Simons, K. and R. Ehehalt (2002).
"Cholesterol, lipid rafts, and disease."
J Clin Invest **110**(5):597-603

Simons, K. and W.L. Vaz (2004).
"Model systems, lipid rafts, and cell membranes."
Annu Rev Biophys Biomol Struct **33**:269-95

Singer, S.J. and G.L. Nicolson (1972).
"The fluid mosaic model of the structure of cell membranes."
Science **175**(23):720-31

Solon, J., O. Gareil, P. Bassereau and Y. Gaudin (2005).
"Membrane deformations induced by the matrix protein of vesicular stomatitis virus in a minimal system."
J Gen Virol **86**(12):3357-63

Stark, W.S., R. Sapp and D. Schilly (1988).
"Rhabdomere turnover and rhodopsin cycle: maintenance of retinula cells in Drosophila melanogaster."
J Neurocytol **17**(4):499-509

Svetina, S. (2007).
"Question 7: The vesicle world: the emergence of cellular life can be related to properties specific to vesicles."
Orig Life Evol Biosph **37**(4-5):445-8

Takimoto, T. and A. Portner (2004).
"Molecular mechanism of paramyxovirus budding."

Virus Res **106**(2):133-45

Tsafrir, I., Y. Caspi, M.A. Guedeau-Boudeville, T. Arzi and J. Stavans (2003).
"Budding and tubulation in highly oblate vesicles by anchored amphiphilic molecules."
Phys Rev Lett **91**(13):138-102

Vigil, A., M.S. Park, O. Martinez, M.A. Chua, S. Xiao, J.F. Cros, L. Martinez-Sobrido, S.L. Woo and A. Garcia-Sastre (2007).
"Use of reverse genetics to enhance the oncolytic properties of Newcastle disease virus."
Cancer Res **67**(17):8285-92

Voeltz, G.K., W.A. Prinz, Y. Shibata, J.M. Rist and T.A. Rapoport (2006).
"A class of membrane proteins shaping the tubular endoplasmic reticulum."
Cell **124**(3):573-86

Welsch, S., B. Muller and H.G. Krausslich (2007).
"More than one door - Budding of enveloped viruses through cellular membranes."
FEBS Lett **581**(11):2089-97

Whittaker, G.R. (2001).
"Intracellular trafficking of influenza virus: clinical implications for molecular medicine."
Expert Rev Mol Med **2001**:1-13

Yamada, E. (1955).
"The fine structure of the renal glomerulus of the mouse."
J Histochem Cytochem **3**(4):30-9

Yanagisawa, M., M. Imai, T. Masui, S. Komura and T. Ohta (2007).
"Growth dynamics of domains in ternary fluid vesicles."
Biophys J **92**(1):115-25

Yusoff, K. and W.S. Tan (2001).
"Newcastle disease virus: macromolecules and opportunities."
Avian Pathology **30**:439– 455

Zimmerberg, J. and M.M. Kozlov (2006).
"How proteins produce cellular membrane curvature."
Nat Rev Mol Cell Biol **7**(1):9-19

APPENDIX I

HOW MUCH OF THE LUV SURFACE SHOULD BE COVERED BY THE M PROTEIN CLUSTER TO PRODUCE THE VESICLE BURSTING?

Let us consider a large unilamellar vesicle (LUV) of the radius R = 50 nm and initial area, S (Figure Appendix A(a)). If the protein clustering induces a cap which has the same curvature as a sphere of the radius R'= 150 nm (Figure Appendix A (b)), the LUV's area covered by this cap may be defined as $S_{new}=S_1+S_2$, where (S1+S2) ≥ S, as shown in Figure Appendix A. The LUV area covered by this cap will increase as a function of the percent of its coverage by the protein. This relationship is shown in the Figure Appendix B. In 1993, Mui and coauthors showed that 3% increase of the initial area of the LUV is enough to produce vesicle bursting. Thus, when S_{new}/S = 1.03 (shown in blue in Figure Appendix B and schematically in A (c)), the bursting of the vesicle takes place. This relationship in areas corresponds to the 10-15% coverage of the LUV area by the protein cap, as can be observed in Figure Appendix B.
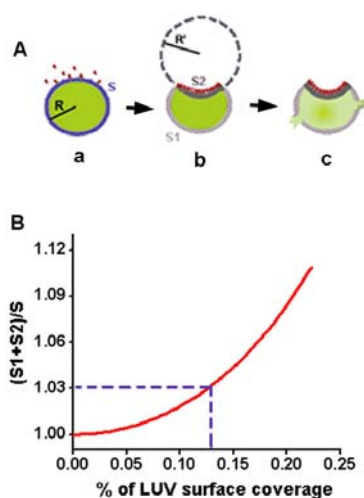

Figure Appendix. A. Schematic representation of the bursting of an LUV induced by the protein cap formation. **B.** The relationship between the LUV surface coverage and the corresponding LUV area increase. LUV radius was assumed to be 50 nm. Protein cap was assumed to have the same curvature as a sphere with the radius of 150 nm.